



UNIVERSITY OF LEEDS

This is a repository copy of *Aggradational lobe fringes: The influence of subtle intrabasinal seabed topography on sediment gravity flow processes and lobe stacking patterns*.

White Rose Research Online URL for this paper:  
<http://eprints.whiterose.ac.uk/103132/>

Version: Accepted Version

---

**Article:**

Spychala, YT, Hodgson, DM [orcid.org/0000-0003-3711-635X](https://orcid.org/0000-0003-3711-635X), Stevenson, CJ et al. (1 more author) (2017) *Aggradational lobe fringes: The influence of subtle intrabasinal seabed topography on sediment gravity flow processes and lobe stacking patterns*. *Sedimentology*, 64 (2). pp. 582-608. ISSN 0037-0746

<https://doi.org/10.1111/sed.12315>

---

© 2016 The Authors. *Sedimentology* © 2016 International Association of Sedimentologists. This is the peer reviewed version of the following article: Spychala, Y. T., Hodgson, D. M., Stevenson, C. J., Flint, S. S. (2017), *Aggradational lobe fringes: The influence of subtle intrabasinal seabed topography on sediment gravity flow processes and lobe stacking patterns*. *Sedimentology*, 64: 582–608. doi: 10.1111/sed.12315, which has been published in final form at [Link to final article using the DOI]. This article may be used for non-commercial purposes in accordance with Wiley Terms and Conditions for Self-Archiving.

**Reuse**

Unless indicated otherwise, fulltext items are protected by copyright with all rights reserved. The copyright exception in section 29 of the Copyright, Designs and Patents Act 1988 allows the making of a single copy solely for the purpose of non-commercial research or private study within the limits of fair dealing. The publisher or other rights-holder may allow further reproduction and re-use of this version - refer to the White Rose Research Online record for this item. Where records identify the publisher as the copyright holder, users can verify any specific terms of use on the publisher's website.

**Takedown**

If you consider content in White Rose Research Online to be in breach of UK law, please notify us by emailing [eprints@whiterose.ac.uk](mailto:eprints@whiterose.ac.uk) including the URL of the record and the reason for the withdrawal request.



[eprints@whiterose.ac.uk](mailto:eprints@whiterose.ac.uk)  
<https://eprints.whiterose.ac.uk/>

Received Date : 25-Sep-2015

Revised Date : 19-Jul-2016

Accepted Date : 27-Jul-2016

Article type : Original Manuscript

## **Aggradational lobe fringes: The influence of subtle intrabasinal seabed topography on sediment gravity flow processes and lobe stacking patterns**

Y.T. Sychala\*, D.M. Hodgson\*, C.J. Stevenson † and S.S. Flint †

\*School of Earth and Environment, University of Leeds, LS2 9JT, UK

† School of Earth, Atmospheric and Environmental Science, University of Manchester, M13 9PL, UK

Correspondence: Yvonne Sychala, School of Earth and Environment, University of Leeds, Leeds, LS2 9JT, UK; E-mail: eeyts@leeds.ac.uk

**Associate Editor – Peter Talling**

**Short Title – Aggradational lobe fringes**

### **ABSTRACT**

Seabed topography is ubiquitous across basin-floor environments, and influences sediment gravity flows and sediment dispersal patterns. The impact of steep (several degrees) confining slopes on sedimentary facies and depositional architecture has been widely documented. However, the influence of gentle (fraction of a degree) confining slopes is less well-documented, largely due to outcrop limitations. Here, exceptional outcrop and research borehole data from Unit A of the Permian Laingsburg Formation, South Africa, provides the means to examine the influence of subtle topography on sediment gravity flow processes and lobe stacking patterns. This is an Accepted Article that has been peer-reviewed and approved for publication in the *Sedimentology*, but has yet to undergo copy-editing and proof correction. Please cite this article as an “Accepted Article”; doi: 10.1111/sed.12315  
This article is protected by copyright. All rights reserved.

lateral confinement on flow behaviour and lobe stacking patterns. The dataset describes the detailed architecture of subunits A.1 to A.6, a succession of stacked lobe complexes, over a palinspastically restored 22 km across-strike transect. Facies distributions, stacking patterns, thickness and palaeoflow trends indicate the presence of a south-east facing low angle (fraction of a degree) lateral intrabasinal slope. Interaction between stratified turbidity currents with a thin basal sand-prone part and a thick mud-prone part and the confining slope result in facies transition from thick-bedded sandstones to thin-bedded heterolithic lobe fringe-type deposits. Slope angle dictates the distance over which the facies transition occurs (hundreds of metres to kilometres). These deposits are stacked vertically over tens of metres in successive lobe complexes to form an aggradational succession of lobe fringe. Extensive slides and debrites are present at the base of lobe complexes, and are associated with steeper restored slope gradients. The persistent facies transition across multiple lobe complexes, and the mass flow deposits, suggests that the intrabasinal slope was dynamic and was never healed by deposition during Unit A times. This study demonstrates the significant influence that even subtle basin-floor topography has on flow behaviour and depositional architecture in the Laingsburg depocentre, Karoo Basin; presenting a new aggradational lobe fringe facies association and recognition criteria for subtle confinement in less well-exposed and subsurface basin fills.

## **Keywords**

Confinement, intrabasinal slope, lobe fringe, remobilisation, submarine lobes, subtle seabed topography.

## **INTRODUCTION**

The behaviour of sedimentary gravity flows is strongly influenced by underlying seabed topography over a wide range of vertical and horizontal scales. Seabed topographic configurations control the general dispersal patterns of sediment and distribution of facies (e.g. Piper & Normark, 1983; Smith & Joseph, 2004; Amy et al., 2004; Smith, 2004a; Twichell et al., 2005; Bersezio et al., 2009; Wynn et al., 2012; Stevenson et al., 2013). The origin of seabed topography may be related to active or inherited tectonic features (e.g. Piper & Normark, 1983; Wilson et al., 1992; Haughton, 2000; Laursen & Normark, 2003; Hodgson & Haughton, 2004; Zakaria et al., 2013; Lin et al., 2014), salt and mud diapirism (e.g. Fusi & Kenyon, 1996; Stewart & Clark, 1999; Rowan et al., 2003; Lopez-Mir et al., 2014), and depositional and erosional relief (e.g. Normark et al., 1979; Pickering & Corregidor, 2005;

Normark et al., 2009; Dakin et al., 2013; Ortiz-Karpf et al., 2015; Spsychala et al., 2015). The impact of static and dynamic seabed topography on depositional architecture and dispersal patterns on the continental slope has been widely documented in subsurface datasets (e.g. Prather et al., 1998; Fiduk et al., 1999; Smith & Møller, 2003; Marchès et al., 2010; Gamberi & Rovere, 2011; Kilhams et al., 2012; Yang & Kim, 2014; Prather et al., 2016). Underlying inherited structures can also exert long-term influence in a basin through differential compaction (e.g. Parker Gay, 1989; Nygård et al., 2002; Færseth and Lien, 2002).

The interaction of turbidity currents and seabed topography results in a wide range of onlap configurations (e.g. Smith & Joseph, 2004; Bersezio et al., 2009; Marini et al., 2015). Understanding sedimentary facies changes and organisation of sub-seismic elements at onlaps can be used to reconstruct the palaeogeographic configurations and tectonic history of sedimentary basins. Smith & Joseph (2004) illustrated a continuum of onlap configurations from abrupt to aggradational onlap as a function of coeval aggradation on the bounding slope and the basin-floor. These authors inferred that abrupt onlaps occur, when little or no coeval sediments are deposited on the slope. Aggradational onlaps occur when aggradation rates on the slope are high associated with a progressive facies change towards the lateral slope (Smith & Joseph, 2004). Smith (2004b) illustrated low-gradient lateral bounding slope scenarios to explain thick intervals of 'lobe fringe' thin-bedded heterolithics, in belts several kilometres wide, adjacent to basin-floor lobe complexes.

The influence of high amplitude palaeo-seabed topography and their associated high degree of confinement on turbidity currents and their depositional architecture is well-constrained from outcrop studies in small basins (Pickering & Hilton, 1998; Sinclair, 2000; Haughton, 2000; Sinclair & Tomasso, 2002, Amy et al., 2004; Hodgson & Haughton, 2004; Smith & Joseph, 2004; Amy et al., 2007; Aas et al., 2010; Etienne, 2012; Etienne et al., 2012; Yang & Kim, 2014; Marini et al., 2015). The angle of confining slopes interpreted from outcrop are commonly higher [for example, 4 to 10° in the Grès d'Annot sub-basins (Puigdefàbregas et al., 2004; Amy et al., 2007); 5 to 10° in the Cengio Turbidite System (Bersezio et al., 2009); >10 to 12° in the Castagnola Turbidite System (Southern et al., 2015)] than the range of slopes identified on reflection seismic and multibeam data (e.g. Gervais et al., 2006; Heiniö & Davies, 2007; Hanquiez et al., 2010; Prather et al., 2012; Stevenson et al., 2013). The effects of confining topography are less well-documented from moderately confined basins (associated with aggradational onlap and bounding slope degrees of <5 to 1°) (Bailleul et al., 2007; Pyles, 2008; Pyles & Jennette, 2009; Burgreen & Graham, 2014) and remain poorly constrained in weakly confined basins (bounding slopes <1°; Smith, 1987a,b; Wilson et al., 1992; Smith, 2004b; Sixsmith et al., 2004), because the recognition of low-gradient slopes requires

inference from isopach and facies trends or exceptionally extensive undeformed outcrops. General recognition criteria were established by Smith (2004 b): (i) palaeoflow parallel to the strike of the palaeoslope; and (ii) lateral replacement of sand-prone lobe complexes by thin-bedded turbidites.

This integrated outcrop and borehole study aims to examine the influence of a gentle lateral intrabasinal slope (fraction of a degree) on the depositional architecture of submarine lobe deposits in Unit A of the Laingsburg Formation, Karoo Basin, South Africa. The objectives are to: (i) examine the distribution of facies associations within the deposits of Unit A; (ii) reconstruct the palaeogeography during deposition; (iii) establish diagnostic criteria for aggradational lobe fringe facies association; and (iv) discuss the implications of the long-term interaction of turbidity currents and seabed topography in a continuum of systems between confined and unconfined settings.

## **GEOLOGICAL AND STRATIGRAPHIC SETTING**

The Karoo Basin has been interpreted as a retroarc foreland basin connected to a magmatic arc and fold-thrust belt (Cape Fold Belt) (Visser & Prackelt, 1996; Visser, 1997; Catuneanu et al., 1998). More recently, Tankard et al. (2009) suggested that subsidence during the early, deep-water, phase of deposition pre-dates the effects of loading by the Cape Fold Belt, and was induced by dynamic topography through mantle flow processes coupled to distant subduction (Pysklywec & Mitrovica, 1999). The basin-fill comprises the Karoo Supergroup and records sedimentation from Late Carboniferous to Early Jurassic. The Karoo Supergroup comprises the glacial Dwyka Group, the deep to shallow-marine Ecca Group and the non-marine/fluvial Beaufort Group. The Ecca Group represents a shallowing-upward succession of sediments from deep-water to fluvial settings (Flint et al., 2011).

### **Stratigraphy of the Laingsburg depocentre**

The Laingsburg depocentre is located in the southwestern part of the Karoo Basin (Fig. 1A). The deep-water stratigraphy comprises mud-prone distal basin-floor fan deposits of the Permian Vischkuil Formation (van der Merwe et al., 2009) overlain by the 550 m thick sand-prone Laingsburg Formation, the focus of this study (Fig. 1B). The Laingsburg Formation is overlain by the Fort Brown Formation, a 400 m thick channelized submarine slope succession (Di Celma et al., 2011; Flint et al., 2011; Hodgson et al., 2011). The Permian Laingsburg Formation is subdivided into Unit A (sand-prone basin floor fan; Sixsmith et al., 2004; Pr elat & Hodgson 2013) and Unit B (base-of-slope

deposits; Grecula et al., 2003; Brunt et al., 2013). A 40 m thick hemipelagic mudstone and (muddy) siltstone separates Units A (up to 300 m) and B (up to 200 m), which contains a thin sand-prone unit referred to as the A/B Interfan (Grecula et al., 2003).

The stratigraphy of Unit A was subdivided by Sixsmith et al. (2004) into seven sandstone-prone subunits called A.1 to A.7 from base to top, separated by regional hemipelagic mudstone horizons. Flint et al. (2011) reassessed the sequence stratigraphy of Unit A through interpretation of relative thicknesses of hemipelagic mudstone and stacking patterns. Unit A comprises three composite sequences. Subunits A.1 to A.3 show a progradational stacking pattern, and together with the overlying hemipelagic mudstone form the first composite sequence. The second composite sequence, which consists of subunits A.4 and A.5 and the overlying hemipelagic mudstone, has the most channel-fills and marks the most basinward advance in sedimentation in Unit A. The third composite sequence includes subunits A.6 and A.7 and with the overlying 40 m-thick mudstone marks an overall retrogradational stacking pattern. The three composite sequences make up the Unit A composite sequence set (Flint et al., 2011). In agreement with Pr lat & Hodgson (2013), subunits A.4 and A.7 have been re-interpreted as lobe complexes within Subunits A.5 and A.6, respectively, because there is no true hemipelagic mudstone separating them (Fig. 1C). Palaeocurrents in Unit A show local complexity, but are dominantly to the north-east (Sixsmith et al., 2004).

## **METHODOLOGY AND DATA SET**

For this study, 21 detailed (1 : 50 scale) bed by bed sections (each ranging from 140 to 300 m), recording grain size, sedimentary structures and bounding surfaces of beds, were measured to establish a south–north strike transect as well as west–east dip-sections to construct correlation panels (Fig. 2). For correlation purposes, facies associations were defined to represent particular sedimentary environments. All correlation panels use the base of Unit A.6 as a datum, because it is present in all outcrops, and the thickness and facies of Unit A.6 shows the least variation over the study area. More than 750 palaeocurrent measurements collected from ripple lamination and tool marks in sandstone beds, and from thrust planes and fold vergence in chaotic and folded deposits, were restored. Outcrop data were integrated with a recently drilled near-outcrop research borehole [Zoutkloof Northern Limb (ZKNL); Figs 2 and 3A to 3G) strategically sited to enhance the existing dataset. For isopach map purposes, thickness data were combined with existing thickness datasets of Unit A (Sixsmith 2000, Sixsmith et al., 2004; Pr lat & Hodgson, 2013).

## **FACIES ASSOCIATIONS**

Unit A is interpreted as a basin-floor fan system composed of tabular sandstone-rich units that are locally cut by sandstone-rich channel-fills (Sixsmith et al., 2004). The sand-rich units (30 to 110 m thick) are laterally extensive (kilometres) and are intercalated with thin-bedded siltstone units. The facies associations, bounding surfaces, and geometrical characteristics are consistent with an interpretation as basin-floor lobe deposits (Prélat et al., 2009), and show a variety of bed thickness patterns controlled by compensational stacking across multiple scales (Prélat & Hodgson, 2013). The basin-floor lobes stack to form lobe complexes (Prélat et al., 2009).

### **Structureless and parallel laminated thick-bedded sandstones (lobe axis)**

This facies association is characterised by thick-bedded (>0.5 to 2.0 m) weakly normally graded upper to lower fine-grained sandstones that are usually structureless but may show faint parallel lamination (Table 1). Bed bases are sharp, loaded or erosional. Beds stack to form 5 to 8 m thick amalgamated units. Amalgamation surfaces are indicated by discontinuous layers of mudclasts or subtle grain-size breaks. In core, dewatering features are common in the lower part of thick sandstone beds. Mudstone clasts are common near bed bases and rarely dispersed through the whole bed. Typically, the sandstone beds are laterally extensive for kilometres (up to 1.5 km) and display tabular geometries. Locally, there is evidence for confinement on a channel-scale such as lenticular geometries, truncation or margin collapse. Some packages of thick-bedded sandstone form large (up to 7 m high) symmetrical deformed features with vertical to overturned bedding that are laterally traceable (over tens of metres) into undeformed successions along the outcrop.

Thick-bedded structureless and parallel laminated sandstone beds are interpreted to be deposited by high density turbidity currents (Kneller & Branney, 1995) with high aggradation rates (Arnott & Hand, 1989; Leclair & Arnott, 2005; Talling et al., 2012). Planar laminations that are produced by high density currents are associated with thick-structureless sandstones. Their geometry, thickness and facies conform to a lobe-axis interpretation (Prélat et al., 2009). Lenticular structureless sandstone beds (100 to 200 m) with basal erosion surfaces are interpreted to be deposited in channel-environments. Scours in Unit A have a more complex geometry and infill (cf. Hofstra et al., 2015). Units with vertical to overturned bedding are interpreted to be formed *in situ* by dewatering (Oliveira et al., 2009).

### **Structured medium to thin bedded sandstone (lobe off-axis)**

Medium to thin-bedded (0.5 to 0.1 m) very fine to fine-grained sandstones display a range of sedimentary structures such as planar, wavy and occasional climbing-ripple lamination (Table 1). Individual beds can preserve more than one type of sedimentary structure. Structureless sandstone beds are rare. Normal grading is common with rare inverse grading observed at bed bases. Two types of hybrid bed are observed in this facies association. (i) Hybrid beds with an upper clast-rich division with a clean sandstone matrix (D3 division of Hodgson, 2009). The clasts are rounded and have a narrow diameter range (<5 cm) within individual beds and located in the upper third of the event bed. (ii) Hybrid beds with an upper banded division (Lowe & Guy, 2000; H2 division of Haughton et al., 2009). Commonly, banded sandstones have a lower structureless division that can make up the bulk of the bed. The banded division comprises alternating light and dark sandstone bands. Darker bands have a clay-rich matrix and are poorly sorted, whereas light bands are quartz-rich and well-sorted. Darker bands can be rich in carbonaceous material and/or mudstone chips. Light bands typically load into the dark bands. There are no grain-size breaks between the individual bands. Observed banded divisions are up to 20 cm thick comprising individual bands each <2 cm thick (see M<sub>2c</sub> and microbanded beds of Lowe & Guy, 2000). Bands are commonly planar or sub-parallel and continuous, but discontinuous bands are also observed. Structured sandstones are extensive for several hundred metres and show tabular geometries in outcrop scale.

Structured medium to thin-bedded sandstones are interpreted to be deposited by low-density turbidity currents. Planar laminations and current ripple-laminations are produced by dilute flows, which rework sediment along the bed (Allen, 1982; Southard, 1991; Best & Bridge, 1992). Where a bed shows repetitive sedimentary structures this may indicate either long lived surging flows or collapsing flows (Jobe et al., 2012). Planar laminations deposited by low density turbidity currents are associated with thin-bedded ripple laminated sandstones. Clean sandstone beds with an upper mud clast rich division are interpreted to be the product of turbidity currents; whereby the head and body of the flows deposit clean sand with mud clasts carried towards the top and rear of the flows, to be deposited on the bed top (Hodgson, 2009). Deposition of banded divisions and their associated lower structureless division is interpreted to be by high-density turbidity currents. The banded division results from fluctuations in clay content in near-bed layers in an aggradational setting as reported during deposition of traction carpets (Lowe, 1982; Sumner et al., 2008; Talling et al., 2012). Deposits are comparable to the H2 division of Haughton et al. (2009) and other transitional flow deposits (Lowe & Guy, 2000; Davis et al., 2009; Fonnesu et al., 2015). The facies and thickness of this association is consistent with an interpretation as deposited in the lobe off-axis (Prélat et al., 2009).

### **Heterolithic packages (lobe fringe)**

Thin-bedded (0.01 to 0.1 m) heterolithic packages (0.2 to 2.5 m thick) (Figs 3F, 4A and 4B; Table 1) comprise fine and coarse siltstones (<5 cm) interbedded with very fine-grained to lower fine-grained sandstone. Sandstone beds contain planar and/or current ripple laminations, with rare climbing ripple lamination. Siltstone beds are either structureless or planar laminated. Bed thickness range is narrow (5 to 10 cm), but 2 to 5 m thick packages with thickening- or thinning-upward trends occur. Two types of hybrid beds (0.05 to 1.5 m thick) are observed within the heterolithic packages. (i) Clean sandstone overlain by an argillaceous (muddy sand) division that is mica-rich and plant material-rich (D1 division of Hodgson, 2009, and H3 division of Haughton et al., 2009). Core observations show that; the fabric in the upper argillaceous division is commonly swirly and patchy. The boundary between the lower and upper division is commonly gradational. Some sand grains in the argillaceous division are coarser than in the underlying sandy division. (ii) Hybrid beds with an upper argillaceous clast-rich division (D2 division of Hodgson, 2009, and H3 division of Haughton et al., 2009). The argillaceous division consists of a muddy sand matrix and subangular to subrounded intraformational mudstone clasts (centimetres to decimetres in size). No preferred orientation of the clasts was observed. The boundary between the lower and upper division can be gradational or sharp. The underlying sandstone can show wavy or pseudo-lamination, when it contains a significant amount of mud chips. Rarely, beds show a lower clean sandstone division overlain by an argillaceous division with either intraformational mudclasts – or a carbonaceous-rich middle division and a clean sandstone upper division (cf. H4 of Haughton et al., 2009).

The heterolithic packages are interpreted as distal, sluggish, dilute flows (Bowen & Stow, 1980; Jobe et al., 2012). Ripple laminations form beneath dilute turbulent flows via reworking of the bed under moderate aggradation rates, whereas climbing-ripple laminations form under high aggradation rates (Allen, 1971; Allen, 1982; Southard, 1991). Hybrid beds are interpreted to be the product of flows that transform along their length from turbidity current to debris flow (Fisher, 1983; Haughton et al., 2009; Fonnesu et al., 2015). The facies and thickness of this association are consistent with an interpretation of a lobe fringe setting (Mutti, 1977; Pickering, 1981; Pr lat et al., 2009).

### **Thin-bedded siltstones (distal lobe fringe)**

This association comprises thin-bedded (0.05 m) fine and coarse siltstones with rare thin (<0.05 m) very fine-grained sandstones (Fig. 4 A and C; Table 1). The siltstones are structureless or planar to starved ripple laminated, when they display a sandy component. Observations from the core show moderate to high bioturbation in these facies associations. Thicknesses of individual intervals are variable (0.5 m to 3.5 m).

Thin-bedded siltstones are the preserved products of dilute turbidity currents. Planar laminated and rippled beds are a product of tractional reworking of the bed (Stow & Piper, 1984; Mutti, 1992; Talling et al., 2012), while structureless beds are a product of direct suspension fallout (Bouma, 1962). The facies is typical of distal lobe fringe environments (Prélat et al., 2009). The variation in interval thicknesses is interpreted to be dependent on the number of overlapping distal lobe fringe deposits (Prélat et al., 2009).

### **Structured climbing bedform dominated heterolithic packages**

Thin-bedded (0.01 to <0.1 m) fine to coarse siltstones are interbedded with sandy siltstones to very fine-grained sandstones (Fig. 5A to E; Table 1). Siltstones make up the bulk of the heterolithic packages (Fig. 5C). Sandstone beds show either planar, stoss-side preserved climbing-ripple or wavy lamination. Ripple morphology is preserved on bed tops, and in cross-section individual beds are sigmoidal with a long thin limb and a shorter thicker limb, used to indicate a palaeoflow direction (Fig.5B). Successions of these ripples form larger dune-like features. The heterolithic package comprises multiple event beds that stack in the direction of palaeoflow (Fig. 5C). Stacking patterns are dominantly aggradational (Fig. 5D). The facies association includes rare hybrid beds with an upper argillaceous carbonaceous division. These heterolithic intervals are up to 10 m thick, and intercalated with thin-bedded siltstone intervals (Fig. 5E).

Structured climbing bed dominated heterolithic packages indicate rapid deposition from dilute turbidity currents. Stoss-side preserved climbing-ripple lamination indicate deposition beneath energetic flows with high aggradation rates forming under high aggradation rates (Allen, 1971; Allen, 1982; Southard, 1991).

### **Chaotic and folded facies association**

Chaotically deformed packages (up to 30 m thick) (Figs. 3B, 3C, 4A, 4D and 4E; Table 1) comprise isoclinal and recumbent folds of thin-bedded (centimetre-scale) siltstones interbedded with very fine-grained sandstones. Where folded, thin-bedded units can be partly disaggregated and encased by a poorly sorted structureless siltstone matrix. Planar, current ripple and climbing-ripple lamination can be observed in beds within the folded sandstone/siltstone packages. In core, the chaotic facies shows micro-faulting (millimetre-scale offsets) around folds (Fig. 3C). Locally, these units are intercalated with relatively undeformed thin-bedded units (Table 1). Bases of chaotic and folded units are sharp to erosive, while bed tops are undulated and irregular.

The orientation of the folds does not conform to the post-depositional tectonic folding of the Laingsburg area stratigraphy. Therefore, the tight folding of the thin-bedded strata is interpreted as syn-depositional deformation due to remobilisation of local thin-bedded stratigraphy. The low amount of disaggregation supports an interpretation of slide deposits, although where the matrix encases clasts of folded thin-beds a debris-flow deposit interpretation is invoked (Woodcock, 1979; Prior et al., 1984; van der Merwe et al., 2009; Talling et al., 2012). Slide deposits and debrites can be followed out for several kilometres and cover an area of at least 65 km<sup>2</sup>.

### **Hemipelagic mudstones**

Mudstones are thin-bedded (0.5 to 1.0 cm) and commonly silty. Mudstone dominated packages can be up to 15 m thick. Concretions are common and can be associated with distinctive horizons in the deposit. Thin-bedded siltstones and ash layers (<5 cm) are locally intercalated. Clastic injection is common, especially in the mudstone horizon that separates Subunits A.5 and A.6 (Cobain et al., 2015). Mudstone packages are regional in extent and do not show thickness changes, except where eroded by remobilized chaotic and folded deposits or flows that deposit younger sand-rich deposits.

Mudstones are interpreted as hemipelagic background deposits; they can be mapped over large areas and mark episodes of sediment starvation to the basin-floor. Flint et al. (2011) interpret these to contain the deep-water expression of maximum flooding surfaces. Mudstone packages therefore serve as useful correlation intervals.

## **PALAEOCURRENTS**

Palaeocurrent measurements show that the mean palaeoflow direction of turbidity currents in Unit A was to the north-east (Fig. 6), consistent with overall north-east to east palaeocurrent measurements in the underlying Upper Vischkuil Formation (van der Merwe et al., 2009) and the overlying Unit B (Brunt et al., 2013) and Fort Brown Formation (Figueiredo et al., 2010; Di Celma et al., 2011; van der Merwe et al., 2014, Spychala et al., 2015). Around Jakkalsfontein and Dapperfontein, palaeocurrents are commonly to the east or show flow patterns to the southeast, especially in subunits A.3 and A.5 (Fig. 6). Palaeocurrent data from ripple laminations in the most northern outcrops (Wilgerhoutfontein 1+2 and Waterkloof) present a narrow spread with a dominant direction to the east. In contrast, measurements of thrust planes and fold vergence from slides indicate transport towards the south-east and south-west (Fig. 6).

## **DISTRIBUTION OF FACIES ASSOCIATIONS AND THEIR THICKNESSES**

In the study area, Unit A comprises six facies associations (Table 1) with five of them representing a particular lobe sub-environment. Pr lat et al. (2009) described ‘lobe axis’, ‘lobe off-axis’, ‘lobe fringe’ and ‘distal lobe fringe’ from detailed mapping of submarine lobes from the nearby Tanqua depocentre. Outcrops in the south of the study area (Skeiding and Rietfontein, Fig. 2) are dominated by lobe axis (Fig. 7A) and lobe off-axis deposits (Sixsmith et al., 2004) separated vertically by lobe fringe associations (Fig. 8). This stratigraphic trend is indicative of compensational stacking patterns (Pr lat & Hodgson 2013). Outcrops in the north of the study area consist of lobe off-axis (Fig. 7B) and fringe deposits intercalated with silt-prone slide deposits and debrites (Doornkloof, Doornfontein and Jakkalsfontein). Slides and debrites occur dominantly at the bases of subunits A.3 and A.5 (Fig. 7D), although thin (<5 m) localised deposits of deformed strata can be observed within the other subunits. Subunit A.3 shows large-scale dewatering structures (up to 7 m high) in its top in the Jakkalsfontein – Dapperfontein area, which are truncated by an overlying debrite at the base of A.5 (Fig. 7C). Climbing-bedform dominated thin-bedded siltstone successions are only present in the northern part of the study area (Waterkloof and Wilgerhoutfontein; Fig. 8). The position of the lateral transition from lobe fringe to climbing thin-bedded siltstones follows a strongly aggradational pattern, with a slight northward trend through the stratigraphy from A.1 to A.6 (Fig. 8). Locally, hemipelagic mudstones between A.2/A.3 and A.3/A.5 are completely removed through entrainment by slides and debris flows in some localities, while the mudstone deposits between A.1/A.2 and A.5/A.6 are preserved across the whole study area (Figs 8, 9 and 10).

In strike section, the thickness of Unit A is 300 m in the south (Skeiding) and thins to 140 m (Jakkalsfontein) towards the north (Fig. 8). Whereas the thickness of subunit A.1 shows no change, A.2 show slight thinning (from *ca* 23 m to *ca* 15 m; Fig. 8), while subunits A.3 to A.5 show a pronounced thinning trend. Subunit A.5, which consists of several lobe complexes, shows the maximum amount of thinning (117 m in the south to 42 m in the north). Subunit A. 3 thins from 43 m to 30 m, whereas A.6 thins slightly from 25 m to 22 m. In depositional dip sections (Fig. 10), subunits A.1 to A.6 maintain a similar thickness, and only minor thickness and facies changes are observed that can be accounted for by compensational stacking at subunit level. Isopach thickness maps (Fig. 10) show an overall shift in the main locus of deposition to the N through A.1 to A.6. Subunit A.3 displays two areas of thicknesses exceeding 30 m. In the south-east, the thickness conforms to lobe deposits, whereas in the north-west the thickness is caused by slides and debrites at the base of A.3 (34 m thick).

## **PALAE GEOGRAPHIC RECONSTRUCTION**

The stratigraphic thinning to the north-west, the presence of mass flow deposits with kinematic evidence of movement to the south-east and south-west, and the thick aggradational succession of climbing ripple dominated thin-bedded siltstone facies with a narrow eastward palaeoflow direction (Fig. 7) in all lobe complexes point to the presence of seabed topography during deposition of Unit A [cf. recognition criteria of low-gradient slopes established by Smith (2004 b)]. Based on these data, a south-west/north-east orientated and south-east facing intrabasinal slope has been reconstructed. The regional palaeocurrent trends in the underlying (Vischkuil Formation) and overlying (Unit B of Laingsburg Formation and Fort Brown Formation) are dominated by overall north-east palaeocurrents (van der Merwe et al., 2009; Brunt et al., 2013; van der Merwe et al., 2014). This indicates that the intrabasinal slope was a lateral slope rather than the main basin margin slope. The limited amount of basinward thickness changes in subunits A.1 to A.6 to the east (Sixsmith et al., 2004; Pr elat & Hodgson 2013, Fig. 9), suggest that the base of the intrabasinal slope ran between Matjiesfontein in the south-west and the centre of the Moordenarskaroo in the north-east (Fig. 10).

The southern study area is characterised by lobe complexes built through compensational stacking of lobes dominated by lobe axis and lobe off-axis deposits intercalated with heterolithic lobe fringe deposits. The northern study area consists of progressively more thin-bedded lobe fringe deposits that show aggradational stacking. Compensational stacking in the south to south-east of the study

area and aggradational stacking in the north-west point to a relatively abrupt change in gradient (Fig. 11), associated with a break in slope.

Slightly more pronounced thinning of A.3 and prominent thinning of A.5 over the transect suggests that the confining slope steepens from the deposition of Subunits A.1 and A.2 to A.3 and A.5. The steepening of the confining slope is coincident with the emplacement of thick slide and debris-flow deposits, which are most abundant in Subunits A.3 and A.5. The slides and debrites comprise remobilised heterolithic stratigraphy (lobe fringe deposits), dominated by thin-bedded climbing ripple laminated sandstones and the regional hemipelagic mudstones. Therefore, it is possible that the increased gradient destabilised sediments that had accumulated on the confining slope. The absence of the regional mudstone *in situ* suggests that remobilisation happened after initiation of subunits A.3 and A.5.

## DISCUSSION

### Aggradational lobe fringe facies association

#### *Flow processes*

Sedimentary structures indicate that very fine-grained sandstones, sandy siltstones, siltstones and mudstones with climbing bedform geometries were deposited rapidly from stratified turbidity currents with a thin basal sand-prone part and a thick mud-prone part. Due to rapid deceleration the upper parts of the flows deposited heterolithic climbing-ripple dominated facies along the intrabasinal slope (Fig. 11). The main sand fraction was partitioned to the south, where lobe complexes display intercalation of dominantly structureless sandstone lobe axes and structured sandstone lobe off-axes with heterolithic lobe fringes that is indicative of unconfined compensational stacking (Fig. 11). The thick sand-rich packages in the south grade abruptly into thin-bedded heterolithic lobe fringe facies in the north-west (against the confining slope). The lateral transition to lobe fringe from lobe axis and off-axis successions supports interpretation of the palaeoenvironment of deposition being stacked lateral lobe fringes (Pickering, 1981, 1983). The lobe fringe facies association in this study differs from the lobe fringe facies association proposed by Pr elat et al. (2009) from the unconfined Tanqua depocentre, largely due to the evidence for high sedimentation rates (climbing ripples and climbing bedforms) and the persistent aggradational stacking of facies over tens of metres on lobe complex scale. The narrow spread of slope sub-parallel palaeocurrents documented within these deposits suggests minor flow deflection (Fig. 6). The term

'aggradational lobe fringes' is proposed here for this specific lobe sub-environment. The lateral facies transition between lobe axis and off-axis to fringe is governed primarily by the height of the topography relative to the thickness of the flows (Muck & Underwood 1990; Pickering & Hilton 1998, Wynn et al., 2012). However, flows are stratified in terms of their grain size and sediment concentration (McCaffrey et al., 2003; Baas et al., 2005; Kane & Pontén, 2012). In relatively unconfined basin-floor settings, flows are likely to be relatively thin; transporting their sandy sediment only meters from the bed with the finer grained component transported in a thicker (tens of metres) dilute overriding layer (Stevenson et al., 2014). The presence of subtle lateral topography on the basin-floor will therefore impose different levels of confinement on the basal and upper parts of the flows (Fig. 11).

#### *Interaction of stratified flows and seabed topography*

A gentle south-east facing lateral slope present during the deposition of A.2, A.3 and A.6 would confine the basal part of the flows (metres thick) and lateral pinching would occur over distances of kilometres. In contrast, the upper parts of flows would be able to easily surmount the topography. This generates a scenario whereby sandy lobe deposition (axis and off-axis environments) is weakly confined by the slope, whilst the fine-grained fringes deposit as if unconfined (Fig. 11A). Fringe deposits from lobes that are deposited further away from the confining slope are extensive. Because they deposit from the dilute part of the flow they will contribute to the deposits on the slope. Therefore, thinning in this scenario is notably gradual (Fig. 11A).

Relatively steeper slopes (subunit A.5) would confine the sandy basal parts of flows more strongly and result in lateral pinching over distances of hundreds of metres. The thicker upper parts of flows are also confined but still onlap higher up the slope and are, therefore, able to deposit drapes onto the bounding slope (cf. Smith & Joseph, 2004). This generates lobe deposits that abruptly (over hundreds of metres) transition into aggradational lobe fringe facies (Fig. 11B). With continued sandy lobe deposition, compensating lobes will stack against the confining slope with aggradational lobe fringes (Fig. 11B).

#### **Nature of the confining structure**

The origin of the lateral slope, and whether it was static or dynamic, is discussed using stratigraphic evidence. The thickness trends and facies distributions (Fig. 10) indicate that the gradient of the confining slope increased through time from A.1 to A.5, then reduced from A.5 to A.6. The persistent lateral facies transition thick aggradationally stacked lobe complex fringes in a similar fashion

indicates that the slope was always present and inhibited the development of lobes. Therefore, the intrabasinal slope was dynamic rather than static. Differential compaction above syn-rift topography has been shown to have a long-lived impact on deep-water sedimentation patterns (e.g. Parker Gay, 1989; Nygård et al., 2002; Færseth & Lien, 2002). However, healing of the slope gradient after the deposition of A.5 indicates that differential compaction above a deeper rigid block cannot be the driving mechanism for the dynamic intrabasinal slope. Syn-tectonic activity deforming the seabed has been postulated previously in the basin (e.g. Grecula et al., 2003; Sixsmith et al., 2014). Sixsmith (2000) proposed syndepositional basin-floor deformation as a driving mechanism for thickness variations, speculating early movement on incipient structures that became the present day east–west trending folds. Sixsmith et al. (2004) inferred that Units A.1 and A.2 pinchout with an onlap against an incipient Hexberg–Bontberg–Heuningberg antiform structure with Unit A.1 and A.2 pinching-out against the structure, and that Unit A thickens dramatically to the north of the Heuningberg anticline. Here, all subunits are correlated over the study area, with no evidence of any subunit pinching out across the Heuningberg anticline area. The thinning and facies trends do not coincide with the present day orientation of fold structures but are consistent with a south-east facing low gradient intrabasinal confining slope.

Timing of mass wasting processes, thickness distributions and slope angles are key indicators to determine the nature of the slope. Mass wasting events have been examined on modern seabed basin margins on slopes gradients as low as 0.05 to 1.4° (Bugge et al., 1988, Masson et al., 1998; Gee et al., 1999; Haflidason et al., 2004; Frey-Martínez et al., 2006). The slides and debrites are located at the bases of Subunits A.3 and A.5 as slope angles increased. It is likely that much of the steepening occurred during the slow accumulation of the hemipelagic drapes that separate Subunit A.2 from A.3 and Subunit A.3 from A.5. The initiation of slides and debris flows may have been due to: (i) oversteepening of the intrabasinal slope; (ii) liquefaction of the underlying muddy deposits (cf. Bull et al., 2009); and (iii) failure through high pore pressure due to high sedimentation rates on the slope (Nygård et al., 2002), or a combination of these processes. Gee et al. (1999) reported that high pore pressures can initiate bed shearing on slopes as little as 0.05° conforming to slope angles during deposition of A.3 and A.5. For example, seismicity can increase slope gradients, liquefy strata and generate overpressure (Heezen & Ewing, 1952; Bugge et al., 1988). Therefore, punctuated mass wasting, and successive steepening of the slope and healing before the deposition of A.6 suggests an underlying tectonic driver and explains the presence of a dynamic if subtle lateral slope, with different rates of tilting and sedimentation governing its gradient at any time on the seabed.

## Estimating the angle of the lateral slope

Estimation of palaeoslope gradients from outcrop data is problematic because many assumptions need to be made. For example, the original gradient of the seabed, the effects of differential sediment compaction, and the amount of post-depositional shortening due to tectonic activity. Although it is not possible to determine original gradient unequivocally, reconstructing an approximate slope gradient is useful in making comparisons across different systems (i.e. low gradient slope <1°; moderate gradient slope 1 to 5°; and high gradient slope <5°). Although the original gradient of the seabed on the basin floor at the time of onset of accumulation of Subunit A1 cannot be determined, it was probably close to zero (van der Merwe et al., 2009). Thinning and facies distribution of Unit A, particularly of remobilised chaotic deposits, suggest that the intrabasinal slope likely dipped to the south-east.

If all the thinning of subunits A.1 to A.6 across the transect from axis to margin is attributed to the presence of a seabed topography, and if the basin floor is assumed to have had no gradient at the time of accumulation, then an approximate minimum intrabasinal slope angle can be estimated using a simple trigonometric approach (see Fig. 11C):

$$\tan^{-1} = (T_{axis} - T_{margin})/d \quad \text{[Equation 1]}$$

Where  $T_{axis}$  is the original accumulated thickness at Rietfontein,  $T_{margin}$  is the original accumulated thickness at Wilgerhoutfontein (for locations see Fig. 2), and  $d$  is the measured distance between the locations (Rietfontein and Wilgerhoutfontein, Fig. 2 along the transect, which has been corrected for post-depositional tectonic shortening (18.7 km current distance; 21.3 km restored distance; Spikings et al., 2015). The results of Eq. 1 have been converted into degrees.

A number of factors need to be taken into consideration when evaluating the uncertainties associated with the reconstruction of slope angles. Firstly, differential compaction will have resulted in significantly reduced thicknesses of the finer-grained lobe fringe deposits compared to the sand-rich lobe successions. Here, preserved section thicknesses have been decompacted using the approach of Sheldon & Retallack (2001) to estimate whether the effects of differential compaction have resulted in a significant error in the calculation of slope angle:

$$C = S_i / [F_o / e^{Dk}] - 1 \quad \text{[Equation 2]}$$

Where  $C$  is the fraction of the original thickness,  $S_i$  is initial solidity,  $F_o$  is the initial porosity,  $D$  is depth of burial in kilometres,  $k$  is the curve-fitting constant. General values for  $S_i$ ,  $F_o$  and  $k$  for marine sediments were established by Sclater & Christie (1980) and Baldwin & Butler (1985). These values

are displayed in Table 2. For sandstone, the following values are used:  $S_i = 0.51$ ,  $F_o = 0.49$ , and  $k = 0.27$  (cf. Sclater & Christie, 1980; Sheldon & Retallack, 2001). Sediments of the Karoo Basin exhibit greenschist metamorphism and were therefore buried to at least 6 km (Tinker et al., 2008; Hansma et al., 2015). The amount of compaction of the sandstone is estimated as follows:

$$C = 0.51/[0.49/e^{6*0.27} - 1] \quad \text{[Equation 3]}$$

This yields a value for  $C$  of 0.55 for sandstone, (i.e. the present preserved thickness has decreased by almost half compared to its original thickness). The values of  $C$  for siltstone and claystone are 0.42 and 0.22, respectively. Lobe axis and off-axis are dominated by sandstone and minor siltstone deposits, whereas lobe fringes are dominated by siltstone and very fine-grained sandstone deposits, and claystone is absent, meaning that decompaction has limited effects on the estimation of slope angle. Table 3 shows compacted and decompact thicknesses, sand percentages and the variation of slope angle for all subunits. Over the whole transect (21.3 km); these thickness variations introduce an average error (variance) in calculated slope gradient of  $\pm 0.01^\circ$  over all subunits.

Second, post-depositional tectonic shortening has reduced the lateral distance of the transect from 21.3 km originally (Spikings et al., 2015) to 18.7 km today ( $d$  in Eq. 1). Spikings et al. (2015) conducted mass-balanced palinspastic restoration of the Laingsburg depocentre, and calculated a post-depositional shortening of 14.2%. Adjacent mass-balanced sections from Laingsburg and Matjiesfontein indicate post-depositional shortening of 14.7% and 9.2%, respectively (Spikings et al., 2015). The range of shortening estimates for the area is 9.2 to 14.7%, which results in corrected lateral distances across the transect ranging from 20.4 to 21.4 km. This 1000 m uncertainty in the amount of shortening corresponds to an error of approximately  $\pm 0.01^\circ$  in slope gradient (Eq. 1; see Table 4).

Using Eq. 1, Subunits A.2 and A.6 experienced slope angles of  $< 0.05^\circ$ , A.3 around  $0.05^\circ$ , whereas A.5 encountered a slope of around  $0.3^\circ$  (see Table 4). Slope angle values for Subunit A.1 fall within the range of error. Nonetheless, the subunit shows palaeoflow directions that are parallel to the inferred slope, suggesting that a slope may have been present at this time of deposition, but the rate of aggradation on the lateral slope was similar to the rate of aggradation on the basin-floor.

## **Grades of confinement and their influence to basin-floor lobe systems**

Several ancient deep marine fans with inferred lateral confinement have been described or inferred, including the Grès d'Annot Formation (south-west Alps, France), the Castagnola Formation and the Cengio Turbidite system (Tertiary Piedmont Basin, Italy), the Mynydd Bach, Aberystwyth, Cwmystwyth and Pysgotwr formations (Welsh Basin, Wales), Laga Formation (South Laga Basin, Central Apennines, Italy) and the Loma de los Baños Formation (Tabernas-Sorbas Basin, Spain). Most of these systems show a range of onlap geometries (Fig. 12).

The Grès d'Annot Formation, the Laga Formation, the Castagnola Formation, the Cengio Turbidite systems and the Loma de los Baños Formation represent systems that were deposited under high to moderate confinement. Lateral palaeoslope values are reported between 4 to 10° (Amy et al., 2007; Salles et al., 2014) for the Grès d'Annot Formation; 6 to 8° (Marini et al., 2015) for the Laga Formation; 10 to 12° for the northern margin of the Castagnola Formation and 4° for the southern margin, respectively (Felletti, 2002; Southern et al., 2015; Marini et al., 2016); and 5 to 10° for the Cengio Turbidite systems (Bersezio et al., 2009; Felletti & Bersezio, 2010). The Grès d'Annot Formation was deposited during the upper Eocene and Oligocene in an Alpine foreland setting. It crops out in synclines of the thrust belt of the south-west Alps in France (Amy et al., 2004). Two styles of onlap (Fig. 12) were described for the sub-basins: (i) abrupt onlap (Sinclair, 2000; Etienne, 2012); and (ii) aggradational onlap with draping of the confining slope (Sinclair, 2000; Etienne, 2012). The Laga Formation was reported to be deposited under changing grades of confinement (confined to semi-confined; Marini et al., 2015) in the Southern Laga Basin, Italy. The termination styles against the lateral slope comprise abrupt onlap and feather-like onlaps of thin ripple-laminated turbidites. The Tertiary Piedmont Basin (Castagnola Formation and Cengio Turbidite systems) developed during the Alpine and Apennine orogenesis as a piggyback basin. Topographic features are complex and comprise several unconformities that resulted in modification of basin size and configuration (Felletti, 2002). Bounding lateral slopes are mostly steep and lead to abrupt onlap, but aggradational onlap has been reported to the southern basin margin with lower slope gradients (4°; Felletti, 2002). The Loma de los Baños Formation, Tabernas-Sorbas Basin, south-east Spain indicates flow confinement against intrabasinal faults, such as the El Cautivo Fault zone (Hodgson & Haughton, 2004). Hodgson & Haughton (2004) reported aggradational onlaps when flows encountered forced folds and abrupt pinch-outs against fault scarps. Several authors (Smith, 1987a,b; Wilson et al., 1992; Smith, 2004b) described an example of subtle topography and its influence on the Welsh Basin Silurian sandstone systems, namely the Mynydd Bach, Aberystwyth, Cwmystwyth and Pysgotwr formations. Sand-prone deposits laterally grade or transition into a mud-rich turbiditic 'levée-like'

constructional feature due to the influence of faults. Smith (2004b) used the geometrical model established by Smith & Joseph (2004) to illustrate the lateral facies change from lobes (Pysgotwr Formation) to thin-bedded heterolithic (Hafdre Formation).

All of the above systems include syndepositional deformed slides/slumps in proximity to the lateral slope. The slides/slumps are interpreted to be initiated through: (i) gravitational instability/re-equilibration of the slope; or (ii) mass dumping of sediment against the slope. Except for the Mynydd Bach Formation, the examples outlined above describe direct onlap of deposits against the confining intrabasinal slopes. In contrast, this study describes a persistent facies transition to 'aggradational lobe fringes' against the confining slope, similar to the facies transitions reported from the Welsh Basin Silurian systems (Smith, 1987a,b; Wilson et al., 1992; Smith, 2004b) and in subsurface from the Ormen Lange turbidite system (Smith & Møller, 2003). The systems discussed exhibit a range of onlap geometries from abrupt to aggradational onlaps, and more subtle facies transitions against the confining slope, which form part of a continuum of possible configurations (Fig. 12).

## CONCLUSIONS

This study uses an integrated outcrop and research borehole data set, from Unit A of the Permian Laingsburg Formation, South Africa, to examine the influence of confinement on flow behaviour, and resulting depositional architecture of basin-floor lobes and lobe complexes. Across strike changes in unit thickness, palaeocurrent patterns and the distribution of sedimentary facies, were combined to reconstruct a laterally confining south-west facing intrabasinal slope. Although subtle, the slope influenced flow behaviour throughout the succession generating distinctive facies distributions over the study area; confining the sandstone-rich deposits to the south, where conventional lobe compensational stacking was able to take place. Against the confining slope, sand-rich lobe facies pinch and transition laterally into thick (tens of metres) aggrading successions of thin-bedded laminated to structureless siltstones, and current/climbing-ripple laminated very fine-grained sandstones: a new facies association termed 'aggradational lobe fringes'. This transition is a result of stratified flows interacting with the slope, whereby sand (transported only metres from the bed) is confined and pinches out, whilst finer-grained sediment is held aloft in a much thicker overriding cloud and deposits much higher up the slope. Distances of facies transition depend on the slope angle. The persistent facies transition across multiple lobe complexes, and the punctuated occurrence of remobilized facies, associated with steeper slope gradients, suggests a tectonically-driven and dynamic intrabasinal slope. This study highlights that basin-floor flows are density

stratified with a thin basal sand-prone part and a thick mud-prone part, meaning that even subtle topography will exert a major influence on lobe architecture. Identification of thick aggradational lobe fringe successions, as a direct response to subtle dynamic intrabasinal topography, widens the range of geometric and facies-based recognition criteria of subtle confinement in basin-floor settings. The framework provided here is important for the improved recognition of lobe confinement in outcrop, and its interpretation in the subsurface.

## **ACKNOWLEDGEMENTS**

Firstly, the authors would like to thank the local farmers for permission to carry out field studies on their land. Further, we would like to thank Sarah Cobain, Riccardo Teloni and Mariana Gomez O'Connell for field assistance. Amandine Pr elat is acknowledged for constructive discussion in the field and of the manuscript. The LOBE 2 project is funded by a major consortium (Anadarko, Bayergas Norge, BG, BHPBilliton, BP, Chevron, DONG Energy, ENGIE, E.ON, Maersk, Marathon, Petrobras, Shell, Statoil, Total, VNG Norge and Woodside). Reviews by the Sedimentology Chief Editor Nigel Mountney and Associate Editor Peter Talling, and the reviewers Fabrizio Felletti and Ru Smith have greatly improved the manuscript.

## **REFERENCES**

- Aas, T.E., Howell, J.A., Janocko, M. and Jackson, C.A.L.** (2010) Control of Aptian palaeobathymetry on turbidite distribution in the Buchan Graben, Outer Moray Firth, Central North Sea. *Mar. Petrol. Geol.*, 27, 412-434.
- Allen, J.R.L.** (1971) Instantaneous sediment deposition rates deduced from climbing-ripple cross-lamination. *J. Geol. Soc. London*, 127, 553-561.
- Allen, J.R.L.** (1982) *Sedimentary Structures: Their Character and Physical Basis*, Vols. 1, 2. Elsevier, Amsterdam, 593pp, 663pp.
- Amy, L.A., McCaffrey, W.D. and Kneller, B.C.** (2004) The influence of a lateral basin-slope on the depositional patterns of natural and experimental turbidity currents. In: *Deep-Water Sedimentation*

*in the Alpine Basin of SE France: New Perspectives on the Grès d'Annot and related systems* (Eds. Joseph, P. and Lomas, S.A.). *Geol. Soc. London Spec. Publ.*, 221,311-330.

**Amy, L.A., Kneller, B.C. and McCaffrey, W.D.** (2007) Facies architecture of the Grès de Peira Cava, SE France: landward stacking patterns in ponded turbiditic basins. *J. Geol. Soc. London*, 164, 143-162.

**Arnott, R.W.C. and Hand, B.C.** (1989) Bedforms, Primary Structures and Grain Fabric in the Presence of Suspended Sediment Rain. *J. Sed. Petrol.*, 59, 1062-1069.

**Baas, J.H., McCaffrey, W.D., Houghton, P.D.W. and Choux, C.** (2005) Coupling between suspended sediment distribution and turbulence structure in a laboratory turbidity current. *J. Geophys. Res.*, 110, 1-20.

**Bailleul, J., Robin, C., Chanier, F., Guillocheau, F., Field, B. and Ferriere, J.** (2007) Turbidite Systems in the Inner Forearc Domain of the Hikurangi Convergent Margin (New Zealand): New Constraints on the Development of Trench-Slope Basins. *J. Sed. Res.*, 77, 263-283.

**Baldwin, B. and Butler, C.O.** (1985) Compaction curves. *AAPG Bulletin*, 69, 622-626.

**Bakke, K., Kane, I.A., Martinsen, O.J., Petersen, S.A., Johansen, T.A., Hustoft, S., Jacobson, F.H. and Groth, A.** (2013) Seismic modelling in the analysis of deep-water sandstone termination styles. *AAPG Bulletin*, 97, 1395-1419.

**Bersezio, R., Felletti, F., Riva, S. and Micucci, L.** (2009) Trends in bed thickness and facies of the turbiditic sandstone bodies: unravelling the effects of basin confinement, depositional processes, and modes of sediment supply. In: *External Controls on the Deep-water Depositional Systems* (Eds. Kneller, B., Martinsen, O.J. and McCaffrey, B.) *SEPM Spec. Publ.*, 92, 303-321.

**Best, J. and Bridge, J.** (1992) The morphology and dynamics of low amplitude bedwaves upon upper stage plane beds and the preservation of planar laminae. *Sedimentology*, 39, 737-752.

**Bouma, A.H.** (1962) Sedimentology of some flysch deposits: a graphic approach to facies interpretation. Elsevier, Amsterdam/New York, 168pp.

**Brunt, R.L., Hodgson, D.M., Flint, S.S., Pringle, J.K., Di Celma, C., Prélat, A. and Grecula, M.** (2013) Confined to unconfined: Anatomy of a base of slope succession, Karoo Basin, South Africa. *Mar. Petrol. Geol.*, 41, 206-221.

**Bugge, T., Belderson, R.H. and Kenyon, N.H.** (1988) The Storegga Slide. *Phil. Trans. Royal Soc. London, Ser. A*, 325, 357-388.

**Bull, S., Cartwright, J. and Huuse, M.** (2009) A subsurface evacuation model for submarine slope failure. *Basin Res.*, 21, 433-443.

**Burgreen, B. and Graham, S.** (2014) Evolution of a deep-water lobe system in the Neogene trench-slope setting of the East Coast Basin, New Zealand: lobe stratigraphy and architecture in a weakly confined basin configuration. *Mar. Petrol. Geol.*, 54, 1-22.

**Catuneanu, O., Hancox, P.J. and Rubidge, B.S.** (1998) Reciprocal flexural behaviour and contrasting stratigraphies: a new basin development model for the Karoo retroarc foreland system, South Africa. *Basin Res.*, 10, 417-439.

**Cobain, S.L., Peakall, J. and Hodgson, D.M.** (2015). Indicators of progradation direction and relative depth in clastic injectites: Implications for laminar versus turbulent flow processes. *Geol. Soc. Am. Bull.*, 127, 1816-1830.

**Collinson, J.D., Martinsen, O., Bakken, B. and Kloster, A.** (1991) Early fill of the Western Irish Namurian Basin: a complex relationship between turbidites and deltas. *Basin Res.*, 3, 223-242.

**Dakin, N., Pickering, K.T., Mohrig, D. and Bayliss, N.J.** (2013) Channel-like features created by erosive submarine debris flows: Field evidence from the Middle Eocene Ainsa Basin, Spanish Pyrenees. *Mar. Petrol. Geol.*, 41, 62-71.

**Davis, C., Haughton, P., McCaffrey, W., Scott, E., Hogg, N. and Kitching, D.** (2009) Character and distribution of hybrid sediment gravity flow deposits from the outer Forties Fan, Palaeocene Central North Sea, UKCS. *Mar. Petrol. Geol.*, 26, 1919-1939.

**Di Celma, C.N., Brunt, R.L., Hodgson, D.M., Flint, S.S. and Kavanagh, J.P.** (2011) Spatial and Temporal Evolution of a Permian Submarine Slope Channel-Levee System, Karoo Basin, South Africa. *J. Sed. Res.*, 81, 579-599.

**Etienne, S.** (2012) Caractérisation architecturale haute-résolution des lobes turbiditiques sableux confinés. Exemple de la Formation des Grès d'Annot (Eocène-Oligocène, SE-France). Unpublished Ph.D. Thesis, Université Bordeaux.

**Etienne, S., Mulder, T., Bez, M., Desaubliaux, G., Kwasniewski, A., Parize, O., Dujoncquoy, E. and Salles, T.** (2012) Multiple scale characterization of sand-rich distal lobe deposit variability: Examples from the Annot Sandstones Formation, Eocene–Oligocene, SE France. *Sed. Geol.*, 273-274, 1-18.

**Faereth, R. B. and Lien, T.** (2002). Cretaceous evolution in the Norwegian Sea—a period characterized by tectonic quiescence. *Mar. Petrol. Geol.*, 19, 1005-1027.

**Felletti, F.** (2002) Complex bedding geometries and facies associations of the turbiditic fill of a confined basin in a transpressive setting (Castagnola Fm., Tertiary Piedmont Basin, NW Italy). *Sedimentology*, 49, 645-667.

**Felletti, F. and Bersezio, R.** (2010) Quantification of the degree of confinement of a turbidite-filled basin: A statistical approach based on bed thickness distribution. *Mar. Petrol. Geol.*, 27, 515-532.

**Fiduk, J.C., Weimer, P., Trudgill, B.D., Rowan, M.G., Gale, P.E., Phair, R.L., Korn, B.E., Roberts, G.R., Gafford, W.T. and Lowe, R.S.** (1999) The Perdido fold belt, northwestern deep Gulf of Mexico, part 2: seismic stratigraphy and petroleum systems. *AAPG Bulletin*, 83, 578-612.

**Figueiredo, J.J.P., Hodgson, D.M., Flint, S.S. and Kavanagh, J.P.** (2010) Depositional Environments and Sequence Stratigraphy of an Exhumed Permian Mudstone-Dominated Submarine Slope Succession, Karoo Basin, South Africa. *J. Sed. Res.*, 80, 97-118.

**Fisher, R.V.** (1983) Flow transformations in sediment gravity flows. *Geology*, 11, 273-274.

**Flint, S.S., Hodgson, D.M., Sprague, A.R., Brunt, R.L., van der Merwe, W.C., Figueiredo, J., Prélat, A., Box, D., Di Celma, C. and Kavanagh, J.P.** (2011) Depositional architecture and sequence stratigraphy of the Karoo basin floor to shelf edge succession, Laingsburg depocentre, South Africa. *Mar. Petrol. Geol.*, 28, 658-674.

**Fonnesu, M., Houghton, P., Felletti, F. and McCaffrey, W.** (2015) Short length-scale variability of hybrid event beds and its applied significance. *Mar. Petrol. Geol.*, 67, 583-603.

**Frey- Martínez, J., Cartwright, J. and James, D.** (2006) Frontally confined versus frontally emergent submarine landslides: A 3D seismic characterisation. *Mar. Petrol. Geol.*, 23, 585-604.

**Fusi, N. and Kenyon, N.H.** (1996) Distribution of mud diapirism and other geological structures from long-range sidescan sonar (GLORIA) data, in the Eastern Mediterranean Sea. *Mar. Geol.*, 132, 21-38.

**Gamberi, F. and Rovere, M.** (2011) Architecture of a modern transient slope fan (Villafranca fan, Gioia basin-Southeastern Tyrrhenian Sea). *Sed. Geol.*, 236, 211-225.

**Gee, M.J.R., Masson, D.G., Watts, A.B. and Allen, P.A.** (1999) The Saharan debris flow: an insight into the mechanics of long runout submarine debris flows. *Sedimentology*, 46, 315-335.

**Gervais, A., Savoye, B., Mulder, T. and Gonthier, E.** (2006) Sandy modern turbidite lobes: A new insight from high resolution seismic data. *Mar. Petrol. Geol.*, 23, 485-502.

**Grech, M., Flint, S., Potts, G., Wickens, D. and Johnson, S.** (2003) Partial Ponding of Turbidite Systems in a Basin with Subtle Growth-fold Topography: Laingsburg-Karoo, South Africa. *J. Sed. Res.*, 73, 603-620.

**Hafliðason, H., Sejrup, H.P., Nygård, A., Mienert, J., Bryn, P., Lien, R., Forsberg, C.F., Berg, K. and Masson, D.** (2004) The Storegga Slide: architecture, geometry and slide development. *Mar. Geol.*, 213, 201-234.

**Hanquiez, V., Mulder, T., Toucanne, S., Lecroart, P., Bonnel, C., Marchès, E. and Gonthier, E. (2010)** The sandy channel-lobe depositional system in the Gulf of Cadiz: Gravity processes forced by contour current processes. *Sed. Geol.*, 229, 110-123.

**Hansma, J., Tohver, E., Schrank, C., Jourdan, F. and Adams, D. (2015)** The timing of the Cape Orogeny: New  $^{40}\text{Ar}/^{39}\text{Ar}$  age constraints on deformation and cooling of the Cape Fold Belt, South Africa. *Gondwana Res.*, 32, 122-137.

**Haughton, P.D.W. (2000)** Evolving turbidite systems on a deforming basin floor, Tabernas, SE Spain. *Sedimentology*, 47, 497-518.

**Haughton, P.D.W., Barker, S.P. and McCaffrey, W.D. (2003)** 'Linked' debrites in sand-rich turbidite systems – origin and significance. *Sedimentology*, 50, 459-482.

**Haughton, P., Davis, C., McCaffrey, W. and Barker, S. (2009)** Hybrid sediment gravity flow deposits – Classification, origin and significance. *Mar. Petrol. Geol.*, 26, 1900-1918.

**Heezen, B.C. and Ewing, M. (1952)** Turbidity currents and submarine slumps, and the 1929 Grand Banks Earthquake. *Am. J. Sci.*, 250, 849-873.

**Heiniö, P. and Davies, R.J. (2007)** Knickpoint migration in submarine channels in response to fold growth, western Niger Delta. *Mar. Petrol. Geol.*, 24, 434-449.

**Hodgson, D.M. (2009)** Distribution and origin of hybrid beds in sand-rich submarine fans of the Tanqua depocentre, Karoo Basin, South Africa. *Mar. Petrol. Geol.*, 26, 1940-1956.

**Hodgson, D.M. and Haughton, P.D.W. (2004)** Impact of syndepositional faulting on gravity current behaviour and deep-water stratigraphy: Tabernas-Sorbas Basin, SE Spain. In: *Confined Turbidite Systems* (Eds. Lomas, S.A. and Joseph, P.) *Geo. Soc. London Spec. Publ.*, 222, pp. 135-158.

**Hodgson, D.M., Di Celma, C.N., Brunt, R.L. and Flint, S.S. (2011)** Submarine slope degradation and aggradation and the stratigraphic evolution of channel-levee systems. *J. Geol. Soc. London*, 168, 625-628.

**Hofstra, M., Hodgson, D.M., Peakall, J. and Flint, S.S.** (2015) Giant-scour fills in ancient channel-lobe transition zones: Formative processes and depositional architecture. *Sed. Geol.*, 329, 98-114.

**Jobe, Z.R., Lowe, D.R. and Morris, W.R.** (2012) Climbing-ripple successions in turbidite systems: depositional environments, sedimentation rates and accumulation times. *Sedimentology*, 59, 867-898.

**Kane, I.A. and Pontén, A.S.M.** (2012) Submarine transitional flow deposits in the Paleogene Gulf of Mexico. *Geology*, 40, 1119-1122.

**Kilhams, B., Hartley, A., Huuse, M. and Davis, C.** (2012) Characterizing the Paleocene turbidites of the North Sea: the Mey Sandstone Member, Lista Formation, UK Central Graben. *Petrol. Geosci.*, 18, 337-354.

**Kneller, B.C. and Branney, M.J.** (1995) Sustained high-density turbidity currents and the deposition of thick massive sands. *Sedimentology*, 42, 607-616.

**Laursen, J. and Normark, W.R.** (2003) Impact of structural and autocyclic basin-floor topography on the depositional evolution of the deep-water Valparaiso forearc basin, central Chile. *Basin Res.*, 15, 201-226.

**Leclair, S.F. and Arnott, R.W.C.** (2005) Parallel Lamination Formed by High-Density Turbidity Currents. *J. Sed. Res.*, 75, 1-5.

**Lin, C., Liu, J., Eriksson, K., Yang, H., Cai, Z., Li, H., Yang, Z. and Rui, Z.** (2014) Late Ordovician, deep-water gravity-flow deposits, palaeogeography and tectonic setting, Tarim Basin, Northwest China. *Basin Res.*, 26, 297-319.

**Lopez-Mir, B., Muñoz, J.A. and Senz, J.G.** (2014). Restoration of basins driven by extension and salt tectonics: Example from the Cotiella Basin in the central Pyrenees. *J. Struct. Geol.*, 69, 147-162.

**Lowe, D.R.** (1982) Sediment Gravity Flows: II Depositional Models with Special Reference to the Deposits of High-Density Turbidity Currents. *J. Sed. Res.*, 52, 279-297.

**Lowe, D.R. and Guy, M.** (2000) Slurry-flow deposits in the Britannia Formation (Lower Cretaceous), North Sea: a new perspective on the turbidity current and debris flow problem. *Sedimentology*, 47, 31-70.

**Marchès, E., Mulder, T., Gonthier, E., Cremer, M., Hanquiez, V., Garlan, T. and Lecroart, P.** (2010) Perched lobe formation in the Gulf of Cadiz: Interactions between gravity processes and contour currents (Algarve Margin, Southern Portugal). *Sed. Geol.*, 229, 81-94.

**Marini, M., Salvatore, M., Ravnås, R. and Moscatelli, M.** (2015) A comparative study of confined vs. semi-confined turbidite lobes from the Lower Messinian Laga Basin (Central Apennines, Italy): Implications for assessment of reservoir architecture. *Mar. Petrol. Geol.*, 63, 142-165.

**Marini, M., Patacci, M., Felletti, F. and McCaffrey, W.D.** (2016) Fill to spill stratigraphic evolution of a confined turbidite mini-basin succession, and its likely well bore expression: The Castagnola Fm, NW Italy. *Mar. Petrol. Geol.*, 69, 94-111.

**Masson, D.G., Canals, M., Alonso, B. Urgeles, R. and Huhnerbach, V.** (1998) The Canary Debris Flow: source area morphology and failure mechanisms. *Sedimentology*, 45, 411-432.

**McCaffrey, W.D., Choux, C.M., Baas, J.H. and Haughton, P.D.W.** (2003) Spatio-temporal evolution of velocity structure, concentration and grain-size stratification within experimental particulate gravity currents. *Mar. Petrol. Geol.*, 20, 851-860.

**Mutti, E.** (1977) Distinctive thin-bedded turbidite facies and related depositional environments in the Eocene Hecho Group (South-central Pyrenees, Spain). *Sedimentology*, 24, 107-131.

**Mutti, E.** (1992). Turbidite Sandstones. Instituto di Geologia, Università di Parma & AGIP, San Donato Milanese, Italy, 275pp.

**Muck, M.T. and Underwood, M.B.** (1990) Upslope flow of turbidity currents: A comparison among field observations, theory, and laboratory models. *Geology*, 18, 54-57.

**Normark, W.R., Paull, C. K., Caress, D.W., Ussler, W. and Silter, R. (2009)** Fine-scale relief related to Late Holocene channel shifting within the floor of the upper Redondo Fan, offshore Southern California, *Sedimentology*, 56, 1690-1704.

**Normark, W.R., Piper, D.J.W. and Hess, G.R. (1979)** Distributary channels, sand lobes, and mesotopography of Navy Submarine Fan, California Borderland, with applications to ancient fan sediments. *Sedimentology*, 26, 749-774.

**Nygård, A., Sejrup, H.P., Hafliðason, H. and King, E.L. (2002)** Geometry and genesis of glacial debris flows on the North Sea Fan: TOBI imagery and deep-tow boomer evidence. *Mar. Geol.*, 188, 15-33.

**Oliveira, C. M., Hodgson, D. M. and Flint, S. S. (2009)** Aseismic controls on in situ soft-sediment deformation processes and products in submarine slope deposits of the Karoo Basin, South Africa. *Sedimentology*, 56, 1201-1225.

**Ortiz-Karpf, A., Hodgson, D.M. and McCaffrey, W.D. (2015)** The role of mass-transport complexes in controlling channel avulsion and the subsequent sediment dispersal patterns on an active margin: The Magdalena Fan, offshore Colombia. *Mar. Petrol. Geol.*, 64, 58-75.

**Parker Gay, S. (1989)** Gravitational Compaction, A Neglected Mechanism in Structural and Stratigraphic Studies: New Evidence from Mid-Continent, USA. *AAPG Bulletin*, 73, 641-657.

**Pickering, K. T. (1981)** Two types of outer fan lobe sequence, from the late Precambrian Kongsfjord Formation submarine fan, Finnmark, North Norway. *J. Sed. Res.*, 51(4).

**Pickering, K. T. (1983)** Transitional submarine fan deposits from the late Precambrian Kongsfjord Formation submarine fan, NE Finnmark, N. Norway. *Sedimentology*, 30(2), 181-199.

**Pickering, K.T. and Corregidor, J.** (2005) Mass-Transport Complexes (MTCs) and Tectonic Control on Basin-Floor Submarine Fans, Middle Eocene, South Spanish Pyrenees. *J. Sed. Res.*, 75, 761-783.

**Pickering, K.T. and Hilton, V.C.** (1998) Turbidite Systems of Southeast France: Application to Hydrocarbon Prospectivity. Vallis Pr., London, 229pp.

**Piper, D.J.W. and Normark, W.R.** (1983) Turbidite depositional patterns and flow characteristics, Navy Submarine Fan, California Borderland, *Sedimentology*, 30, 681-694.

**Prather, B.E., Booth, J.R., Steffens, G.S. and Craig, P.A.** (1998) Classification, Lithologic Calibration, and Stratigraphic Succession of Seismic Facies of Intraslope Basins, Deep-Water Gulf of Mexico. *AAPG Bulletin*, 82, 701-728.

**Prather, B.E., Pirmez, C., Sylvester, Z. and Prather, D.S.** (2012) Stratigraphic Response to Evolving Geomorphology in a Submarine Apron Perched on the Upper Niger Delta Slope. In: *Application of the Principles of Seismic Geomorphology to Continental -Slope and Base-of-Slope Systems: Case Studies from Seafloor and Near-Seafloor Analogues* (Eds. Prather, B.E., Deptuck, M.E., Mohrig, D., van Hoorn, B. and Wynn, R.B.). *SEPM Spec. Publ.*, 99, pp. 145-161.

**Prather, B.E., O'Byrne, C., Pirmez, C. and Sylvester, Z.** (2016) Sediment Partitioning, Continental Slopes and Base-of-slope Systems. *Basin Res.*, DOI: 10.1111/bre.12190

**Prélat, A. and Hodgson, D.M.** (2013) The full range of turbidite bed thickness patterns in submarine lobes: controls and implications. *J. Geol. Soc. London*, 170, 1-6.

**Prélat, A., Hodgson, D.M. and Flint, S.S.** (2009) Evolution, architecture and hierarchy of distributary deep-water deposits: a high-resolution outcrop investigation from the Permian Karoo Basin, South Africa. *Sedimentology*, 56, 2132-2154.

**Prior, D.B., Bornhold, B.D. and Johns, M.W.** (1984) Depositional characteristics of a submarine debris-flow. *J. Geol.*, 92, 707-727.

**Puigdefàbregas, C., Gjelberg, J. and Vaksdal, M.** (2004) The Grès d'Annot in the Annot syncline: outer basin-margin onlap and associated soft-sediment deformation. In: *Deep-Water Sedimentation in the Alpine Basin of Se France: New Perspectives on the Gres d'Annot and related systems*. (Eds. Joseph, P. and Lomas, S.A.) *Geol.Soc. London Spec. Publ.*, 221, pp. 367-388.

**Pysklywec, R.N. and Mitrovica, J.X.** (1999) The Role of Subduction-Induced Subsidence in the Evolution of the Karoo Basin. *J. Geol.*, 107, 155-164.

**Rowan, M.G., Lawton, T.F., Giles, K.A. and Ratliff, R.A.** (2003) Near-salt deformation in La Popa basin, Mexico, and the northern Gulf of Mexico: A general model for passive diapirism. *AAPG Bulletin*, 87, 733-756.

**Salles, L., Ford, M. and Joseph, P.** (2014) Characteristics of axially-sourced turbidite sedimentation on an active wedge-top basin (Annot Sandstone, SE France). *Mar. Petrol. Geol.*, 56, 305-323.

**Slater, P.A.F. and Christie, J.G.** (1980) Continental stretching: an explanation of the post-mid-Cretaceous subsidence of the central North Sea basin. *J. Geophys. Res.*, 85, 3711-3739.

**Sheldon, N.D. and Retallack, G.J.** (2001) Equation for compaction of paleosols due to burial. *Geology*, 29, 247-250.

**Sinclair, H.D.** (2000) Delta-Fed Turbidites Infilling Topographically Complex Basins: A New Depositional Model for the Annot Sandstones, SE France. *J. Sed. Res.*, 70, 504-519.

**Sinclair, H.D. and Tomasso, M.** (2002) Depositional evolution of confined turbidite basins. *J. Sed. Res.*, 72, 451-456.

**Sixsmith, P.J.** (2000) Stratigraphic development of a Permian turbidite system on a deforming basin floor: Laingsburg Formation, Karoo basin, South Africa. Unpublished Ph.D. thesis, University of Liverpool.

**Sixsmith, P.J., Flint, S.S., Wickens, H.D. and Johnson, S.D.** (2004) Anatomy and Stratigraphic Development of a Basin Floor Turbidite System in the Laingsburg Formation, Main Karoo Basin, South Africa. *J. Sed. Res.*, 74, 239-254.

**Smith, R.D.A.** (1987 a) Structure and deformation history of the Central Wales Synclinorium, northeast Dyfed: evidence for a long-lived basement structure. *Geol. J.*, 22, 183-198.

**Smith, R.D.A.** (1987 b) The *griestoniensis* zone turbidite system, Welsh Basin. In: Marine Clastic Sedimentology: Concepts and Case Studies (Eds. Leggett, J.K. and Zuffa, G.G.) *Graham and Trotman*, London, 89-107.

**Smith, R.** (2004 a) Silled sub-basins to connected tortuous corridors: Sediment distribution systems on topographically complex sub-aqueous slopes. In: *Confined Turbidite Systems* (Ed. Lomas, S.A.) *Geol. Soc. London Spec. Publ.*, 222, 23-43.

**Smith, R.** (2004 b) Turbidite systems influenced by structurally induced topography in the multi-sourced Welsh Basin. In: *Confined Turbidite Systems* (Ed. Lomas, S.A.) *Geol. Soc. London Spec. Publ.*, 222, 209-228.

**Smith, R. and Møller, N.** (2003) Sedimentology and reservoir modelling of the Ormen Lange field, mid Norway. *Mar. Petrol. Geol.*, 20, 601-613.

**Smith, R. and Joseph, P.** (2004) Onlap stratal architectures in the Gres d'Annot: geometric models and controlling factors. In: *Deep-Water Sedimentation in the Alpine Basin of Se France: New Perspectives on the Gres d'Annot and related systems.* (Eds. Joseph, P. and Lomas, S.A.) *Geol. Soc. London Spec. Publ.*, 221, pp. 389-399.

**Southard, J.B.** (1991) Experimental determination of bed-Form stability. *Ann. Rev. Earth Pl. Sc.*, 19, 423-55.

**Southern, S., Patacci, M., Felletti, F. and McCaffrey, W.D.** (2015) Influence of flow containment and substrate entrainment upon sandy hybrid event beds containing a co-genetic mud-clast-rich division. *Sed. Geol.*, 321, 105-122.

**Spikings, A.L., Hodgson, D.M., Paton, D.A. and Spychala, Y.T.** (2015) Palinspastic restoration of an exhumed deep-water system: a workflow to improve paleogeographic reconstructions. *SEG Interpretation*, 3 (4), SAA71-SAA87.

**Spychala, Y.T., Hodgson, D.M., Flint, S.S. and Mountney, N.P.** (2015) Constraining the sedimentology and stratigraphy of submarine intraslope lobe deposits using exhumed examples from the Karoo Basin, South Africa. *Sed. Geol.*, 322, 67-81.

**Stevenson, C.J., Talling, P.J., Wynn, R.B., Masson, D.G., Hunt, J.E., Fren, M., Akhmetzhanov, A. and Cronin, B.T.** (2013) The flows that left no trace: investigating very large-volume turbidity currents that bypassed sediment through submarine channels without eroding the seafloor. *Mar. Petrol. Geol.*, 41, 186-205.

**Stevenson, C.J., Talling, P.J., Sumner, E.J., Masson, D.G., Frenz, M. and Wynn, R.B.** (2014) On how thin submarine flows transported large volumes of sand for hundreds of kilometres across a flat basin plain without eroding the sea floor. *Sedimentology*, 61, pp.1982-2019.

**Stewart, S.A. and Clark, J.A.** (1999) Impact of salt on the structure of the Central North Sea hydrocarbon fairways. *Petroleum Geology Conference series*, 5, 179- 200.

**Stow, D.A.V. and Bowen, A.J.** (1980) A physical model for the transport and sorting of fine-grained sediment by turbidity currents. *Sedimentology*, 27, 31-46.

**Stow, D.A.V. and Piper, D.J.W.** (1984) Deep-water fine-grained sediments: facies models. In: Fine-grained Sediments: Deep-water Processes and Facies (Eds. Stow, D.A.V. and Piper, D.J.W.). *Geol. Soc. London Spec. Publ.*, 15, pp. 611-646.

**Sumner, E.J., Amy, L.A. and Talling, P.J.** (2008) Deposit Structure and Processes of Sand Deposition from Decelerating Sediment Suspensions. *J. Sed. Res.*, 79, 529-547.

**Talling, P.J., Masson, D.G., Sumner, E.J. and Malgesini, G.** (2012) Subaqueous sediment density flows: Depositional processes and deposit types. *Sedimentology*, 59, 1937-2003.

**Tankard, A., Welsink, H., Aukes, P., Newton, R. and Stettler, E.** (2009) Tectonic evolution of the Cape and Karoo basins of South Africa. *Mar. Petrol. Geol.*, 26, 1379-1412.

**Tinker, J., de Wit, M. and Brown, R.** (2008) Mesozoic exhumation of the southern Cape, South Africa, quantified using apatite fission track thermochronology. *Tectonophysics*, 455, 77-93.

**Twichell, D.C., Cross, V.A., Hanson, A.D., Buck, B.J., Zybala, J.G. and Rudin, M.J.** (2005) Seismic Architecture and Lithofacies of Turbidites in Lake Mead (Arizona and Nevada, U.S.A.), an Analogue for Topographically Complex Basins. *J. Sed. Res.*, 75, 134-148.

**van der Merwe, W.C., Hodgson, D.M. and Flint, S.S.** (2009) Widespread syn-sedimentary deformation on a muddy deep-water basin-floor: the Vischkuil Formation (Permian), Karoo Basin, South Africa. *Basin Res.*, 21, 389-406.

**van der Merwe, W.C., Hodgson, D.M., Brunt, R.L. and Flint, S.S.** (2014) Depositional architecture of sand-attached and sand-detached channel-lobe transition zones on an exhumed stepped slope mapped over a 2500 km<sup>2</sup> area. *Geosphere*, 10, 1076-1093.

**Visser, J.N.J.** (1997) Deglaciation sequences in the Permo-Carboniferous Karoo and Kalahari basins of the southern Africa: a toll in the analysis of cyclic glaciomarine basin fills. *Sedimentology*, 44, 507-521.

**Visser, J.N.J. and Prackelt, H.E.** (1996) Subduction, mega-shear systems and Late Palaeozoic basin development in the African segment of Gondwana. *Geol. Rundsch.*, 85, 632-646.

**Wilson, D., Davies, J.R., Waters, R.A. and Zalasiewicz, J.A.** (1992) A fault-controlled depositional model for the Aberystwyth Grits turbiditic system. *Geol. Mag.*, 129, 595-607.

**Woodcock, N.H.** (1979) Sizes of submarine slides and their significance. *J. Struct. Geol.*, 1, 137-142.

**Wynn, R.B., Talling, P.J., Masson, D.G., Le Bas, T.P., Cronin, B.T. and Stevenson, C.J.** (2012) The Influence of Subtle Gradient Changes on Deep-Water Gravity Flows: A Case Study from the Moroccan Turbidite System. In: *Application of the Principles of Seismic Geomorphology to Continental-Slope and Base-of-Slope Systems: Case Studies from Seafloor and Near-Seafloor Analogues* (Eds. Prather, B.E., Deptuck, M.E., Mohrig, D., Van Hoorn, B. and Wynn, R.B.), *SEPM Spec. Publ.*, 99, pp. 347-369.

**Yang, S.-Y. and Kim, J.W.** (2014) Pliocene basin-floor fan sedimentation in the Bay of Bengal (offshore northwest Myanmar). *Mar. Petrol. Geol.*, 49, 45-58.

**Zakaria, A.A., Johnson, H.D., Jackson, C.A.L. and Tongkul, F.** (2013) Sedimentary facies analysis and depositional model of the Palaeogene West Crocker submarine fan system, NW Borneo. *J. Asian Earth Sci.*, 76, 283-300.

## FIGURE CAPTIONS

Table 1. Observed facies associations in Unit A and their appearance in outcrop and core. Items used for scale in photographic panels are: compass in 1 and 3 is 11 cm; lense cap in 2 and 6 is 7 cm; part of logging pole in 4 is 15 cm; logging pole increments in 5 are 10 cm.

Table 2. Constants for compaction equation (Eq. 2).  $S_i$  is initial solidity,  $F_o$  is the initial porosity,  $D$  is depth of burial in kilometres,  $k$  ( $\times 10^{-5} \text{cm}^{-1}$ ) is the curve-fitting constant and  $C$  is the fraction of the original thickness. Values are taken from Sclater & Christie (1980).

Table 3. Compacted and decompacted thicknesses and corresponding slope angles. Slope angles have been calculated using Eq. 1 with a calculated shortening of the transect of 14.2%, i.e. 21.3 km for distance.

Table 4. Effects of 9.2%, 14.2% and 14.7% tectonic shortening on estimated slope angles. Slope angles have been calculated using Eq. 1. Note: Thicknesses for the estimations are decompacted thicknesses (see Table 3).

Fig. 1. (A) The Laingsburg depocentre inboard of the Cape Fold Belt. The blue dashed square indicates the area of study. (B) Stratigraphy of the Laingsburg depocentre. The Laingsburg Formation

overlies the Vischkuil Formation and is overlain by the Fort Brown Formation (Flint et al., 2011). (C) Unit A comprises six subunits, separated by regional hemipelagic mudstone horizons (modified from Sixsmith et al., 2004). Images taken from Google Earth.

Fig. 2. Log locations and lines of correlated sections. The grey line indicates the south–north transect (Fig. 9), blue, violet, green (Fig. 10) and beige lines indicate dip-section correlation panels. Black dots indicate logged sections, blue dot the location of the Zoutkloof Northern Limb (ZKNL) core.

Fig. 3. Zoutkloof Northern Limb (ZKNL) core log and photographs. (A) Core log through Subunit A.5 (B) Mud-streak rich sandstone on the top of A.3. Coin as scale (*ca* 1 cm diameter). (C) Silt-prone syndepositional deformed interval of the chaotic facies. Coin as scale (*ca* 1 cm diameter). (D) Clean sandstone loading into a debritic top of a hybrid bed. Coin as scale (*ca* 1 cm diameter). (E) Dewatering features in a sandstone. Coin as scale (*ca* 1 cm). (F) Ripple-laminated sandstones intercalated with siltstone deposits. Coin as scale (*ca* 1 cm diameter). (G) Highly sheared siltstone-prone package. Coin as scale (*ca* 1 cm diameter).

Fig. 4. (A) Sedimentary log through Doornkloof 1 section (see Fig. 3). Expanded parts show slide facies and lobe fringe facies. (B) Thin-bedded appearance of A.1 at the lateral lobe complex margin at Steekweglagte 1. Logging pole for scale. (C) Lobe fringe deposits of Subunit A.1. Pencil (*ca* 15 cm) for scale. (D) Slightly deformed thin-beds in the Jakkalsfontein area. Geologist for scale (1.65 m). (E) View into the Doornkloof area.

Fig. 5. (A) Sedimentary log of the Wilgerhoutfontein 2 section (see Fig. 3). Representative photographs to show the appearance of the aggradational lobe facies association (logging pole for scale). (B) Very fine-grained sandstone beds showing sigmoidal shapes. Logging pole for scale. (C) Package of climbing siltstone beds. Note the trajectory indicating flow direction. Compass for scale. (D) Very fine-grained sandstone dominated package, climbing ripple laminated. Logging pole for scale. (E) Thin-bedded planar laminated coarse siltstones.

Fig. 6. Palaeocurrents for Unit A (cumulative) and subunits A.1 to A.6. Black: palaeocurrents for lobe deposits; blue: movement direction for chaotic deposits. Orange line: mean palaeoflow direction of lobe deposits; blue line: mean movement direction of chaotic deposits.

Fig. 7. Representative photographs for Unit A, Laingsburg Formation. (A) Thick-bedded structureless sandstones dominated by lobe axis deposits separated by lobe fringe thin-beds indicating compensational stacking in the southwestern study area (Rietfontein). Geologist (*ca* 1.65 m) for scale. (B) Medium-bedded structures sandstones interbedded with heterolithic packages in the northern study area (Jakkalsfontein). Geologist (*ca* 1.65 m) for scale. (C) Large-scale dewatering

feature at Jakkalsfontein 1 in A.3. The flames are truncated by an erosion surface overlain by a debrite at the base of A.5. Geologist as scale (*ca* 1.7 m). (D) Photographic panel of the Jakkalsfontein area showing Subunits A.5 and A.6. Both subunits have a basal slide deposit that is overlain by bedded sandstones. The base of the A.5 slide is erosive and truncated the big-scale dewatering features at the top of A.3.

Fig. 8. South–north transect correlation panels. Top: Correlation of subunits. Unit A thins to the north from *ca* 270 m to *ca* 160 m. Middle: Correlation of lobe sub-environments. Slide deposits occur in the Doornfontein and Jakkalsfontein areas. In the most northerly outcrop all facies associations are replaced by the aggradational lobe fringe facies association: SK2 – Skeiding 2; RF – Rietfontein; DF – Doornfontein 1; JF 1 – Jakkalsfontein 1; WHF – Wilgerhoutfontein. (B) Southern Heuningberg anticline correlation panel: DPF – Dapperfontein; JF – Jakkalsfontein. Fig. 3 shows locations of transects. Bottom: Percentage of facies proportion over the transect. Note that at Wilgerhoutfontein the typical lobe environments are replaced by 'aggradational lobe fringe' facies.

Fig. 9. West–east transect (down-dip) correlation panel from the Doornkloof-Doornfontein area. Note that thickness remains the almost the same over 5.6 km. Slight thickness changes are due to compensational stacking of the subunits.

Fig. 10. Thickness isopach and palaeoenvironmental maps for subunits A.1 to A.6. Note that A.1 and A.2 do not show specific thickness trends but do show facies trends. A.3 to A.6 thin above a south-east facing slope: DF – Doornfontein; DK – Doornkloof; GB – Geelbeck; JF – Jakkalsfontein; SK – Skeidingen; SWL – Steegweglagte; WH – Wilgerhout; WHF – Wilgerhoutfontein; ZKNL – Zoutkloof Northern Limb; MF – Matjiesfontein. Black boxes show the main study area.

Fig. 11. Schematic evolution of lobes and stacking patterns within subunits (thicknesses exaggerated). (A) With a gentle intrabasinal slope as during the deposition of A.3 compensational stacking pattern in the main depocentre passes into a mixed aggradational and distal fringe on the slope. The transition from lobe axis and off-axis deposits to aggradational fringe deposits occurs over kilometres (climbing trajectory). (B) A relative steeper intrabasinal slope as present during deposition of A.5 results in compensational stacking in the main depocentre and abrupt facies transitions (hundreds of metres; vertical trajectory) and thinning to the slope, where aggradational fringe and distal lobe fringe deposits are successively located slope-upwards. (C) Estimation of slope angle using trigonometric geometries. Where  $T_{axis}$  is the thickness at Rietfontein,  $T_{margin}$  is the

thickness at Wilgerhoutfontein (for locations see Fig. 2), and  $d$  is the distance between the locations (18.7 km) along the transect corrected for post-depositional tectonic shortening.

Fig. 12. Submarine basin-floor lobes and their interaction with topographic features: (i) low amount of aggradation on the slope compared to the basin – abrupt pinch-out against structure; (ii) moderate amount of aggradation on the slope compared to the basin – aggradational onlap with draping muds; (iii) low-gradient slope and high aggradation rates – facies transition and remobilisation; and (iv) unconfined – downlap.

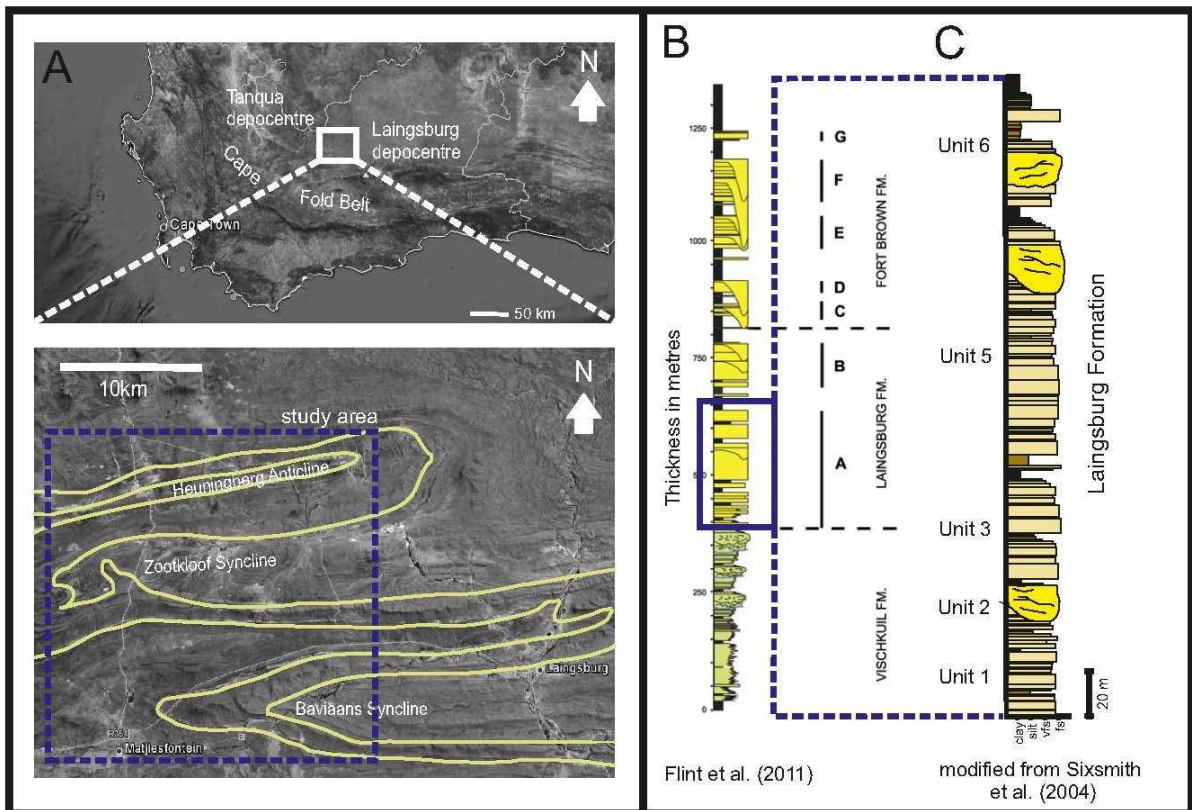
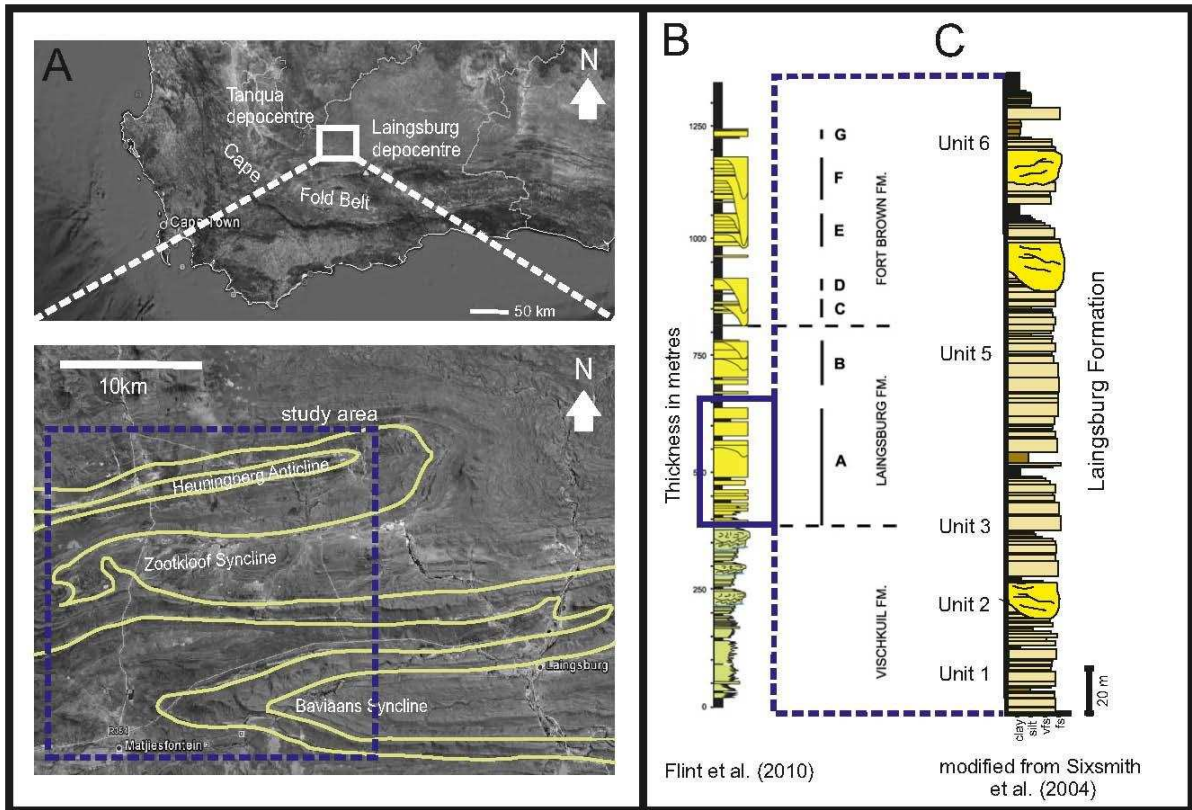
**Table 1**  
Description of the facies associations defined in Unit A

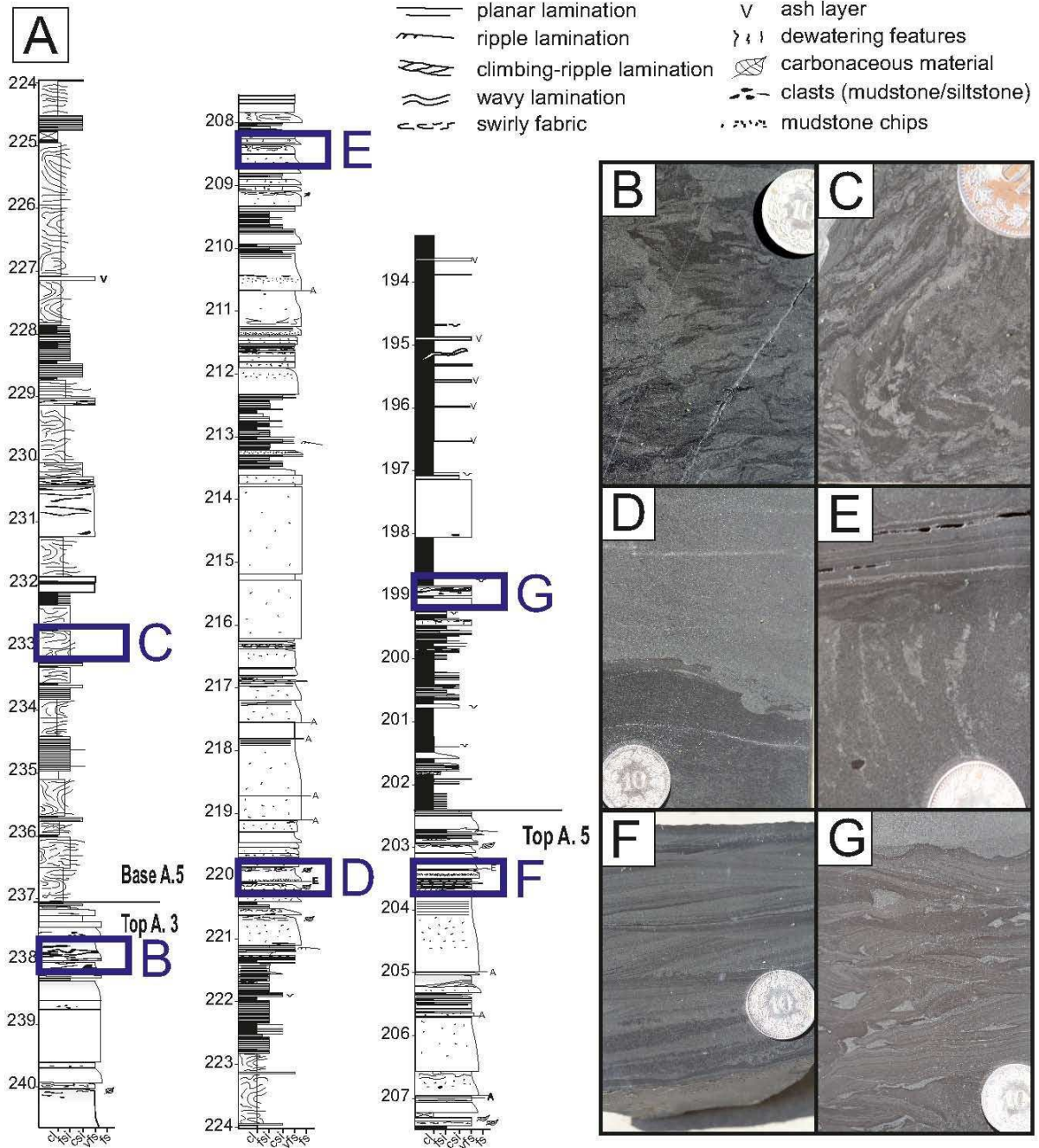
Facies association	Description	
1. Lobe- axis	thick bedded (0.5m - 2m) lower fine to upper fine sandstones structureless, dewatering features highly amalgamated occasionally faint lamination	
2. Lobe off-axis	medium to thin bedded (0.1m - 0.5 m) very fine to lower fine sandstones planar, ripple/ climbing ripple or wavy laminations generally normal graded, sometimes inverse grading hybrid beds with upper banded division or upper clast division	
3. Lobe fringe	thin-bedded (<0.1 m) heterolithic packages planar, ripple/climbing ripple lamination hybrid beds with upper carbonaceous or upper argillaceous clast-rich division	
4. Lobe distal fringe	thin-bedded (<0.1 m) fine to coarse siltstone mostly planar laminated sometimes with small scale ripples (< 1cm)	
5. Aggradational lobe fringe	thin-bedded (<0.1 m) siltstone, sandy siltstone and very fine sandstone dominant ripple laminated, minor planar and wavy lamination sigmoidal (or climbing) bedforms occasionally hybrid beds with upper argillaceous clast-rich division	
6. Chaotic facies	silt-prone matrix with intraformational clasts/ sandy slumps intraformational mudstone clasts consist of folded coarse siltstone to very fine sandstone; folds are isoclinal or recumbent folded erosive based	

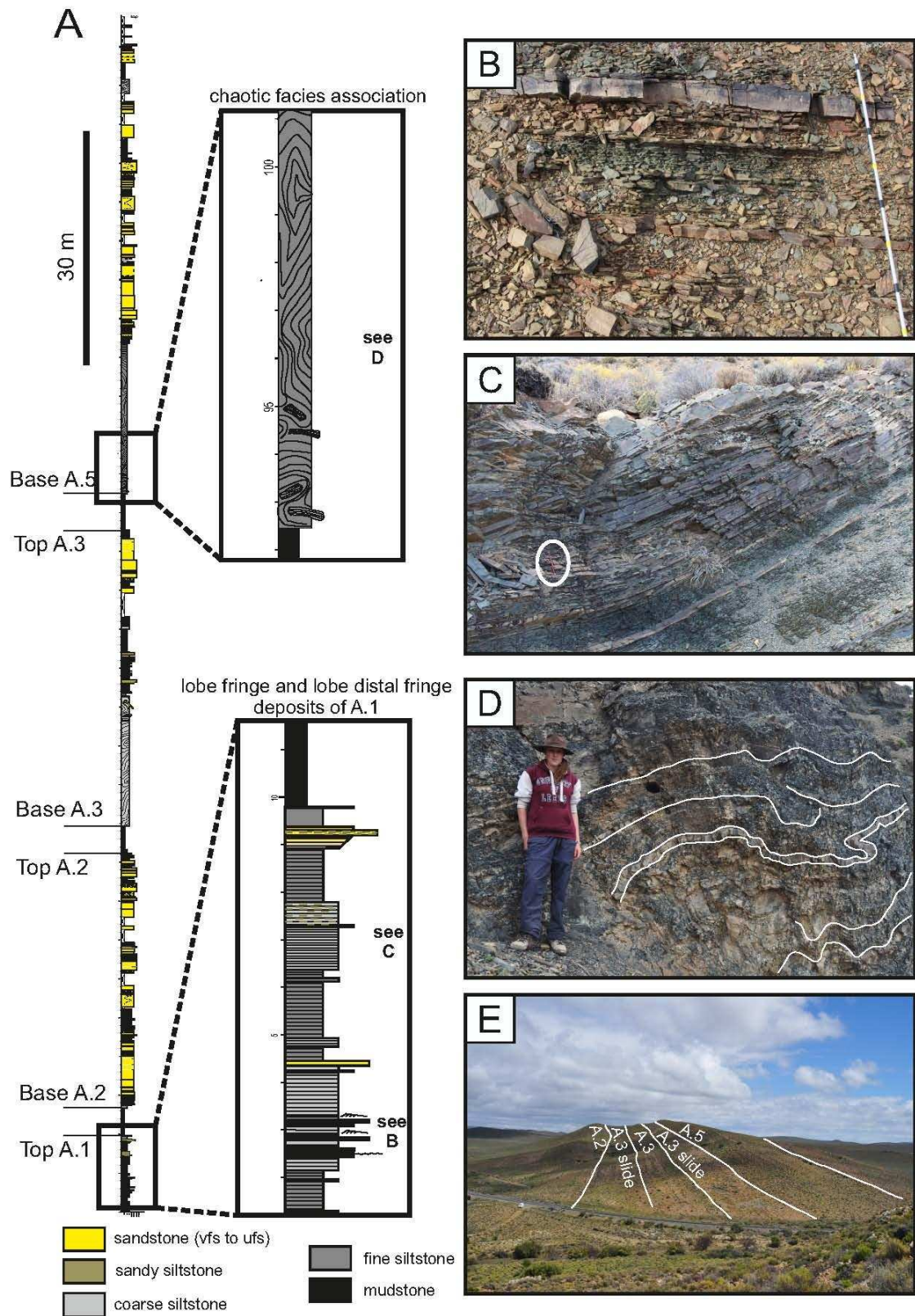
Constants for compaction equation					
Lithology	$S_i$	$F_o$	$k$	$D$	$C$
Sandstone	0.51	0.49	0.27	6 km	0.55
Siltstone	0.44	0.56	0.39	6 km	0.42
Claystone	0.21	0.63	0.51	6 km	0.22

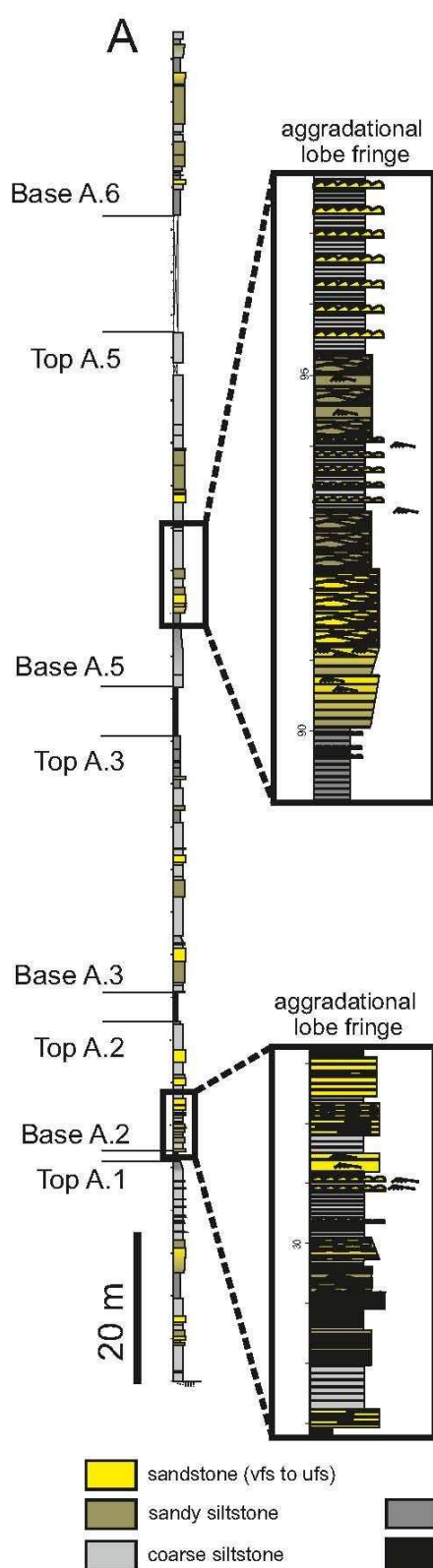
<b>Compacted and decompacted thicknesses and corresponding slope gradients</b>					
	<b>A.1</b>	<b>A.2</b>	<b>A.3</b>	<b>A.5</b>	<b>A.6</b>
Sandstone % (axis/margin)	63/25	77/54	84/46	83/33	92/55
Siltstone % (axis/margin)	37/75	23/46	16/54	17/67	8/45
Measured thickness Rietfontein [m]	21.7	22.5	42.7	116.9	24.9
Measured thickness Wilgerhoutfontein [m]	23.7	15.2	30	41.8	21.9
Compacted Taxis-Tmargin [m]	-2	7.3	12.7	75.1	3
Estimated compacted slope angle [°]	n.a.	0.02	0.03	0.2	0.01
Decompacted thickness Rietfontein [m]	32.5	33.3	62.8	172.2	36.3
Decompacted thickness Wilgerhoutfontein [m]	36.6	22.9	45.6	64.3	33
Decompacted Taxis-Tmargin [m]	-4.1	11	17.2	107.9	3.3
Estimated decompacted slope angle [°]	n.a.	0.03	0.05	0.29	0.01

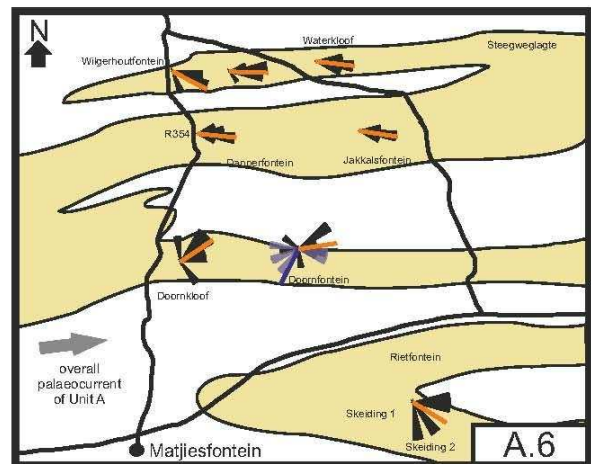
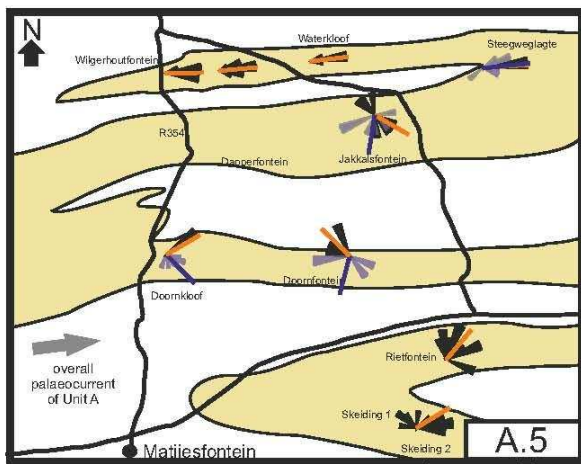
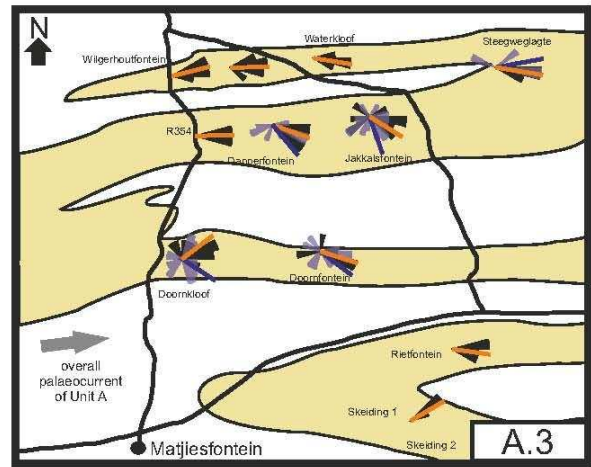
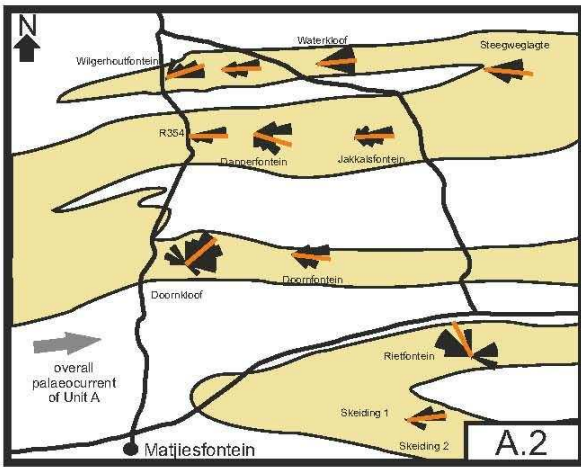
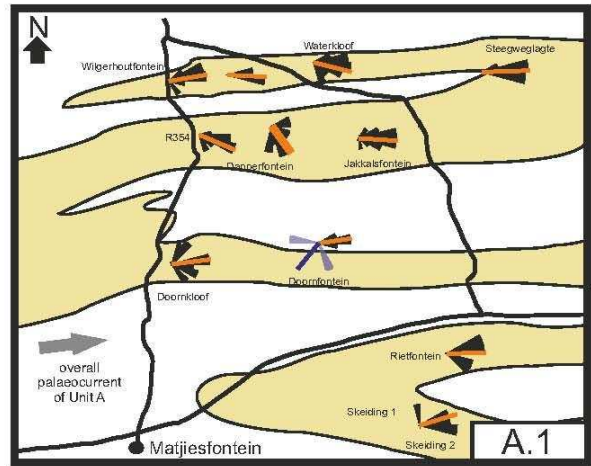
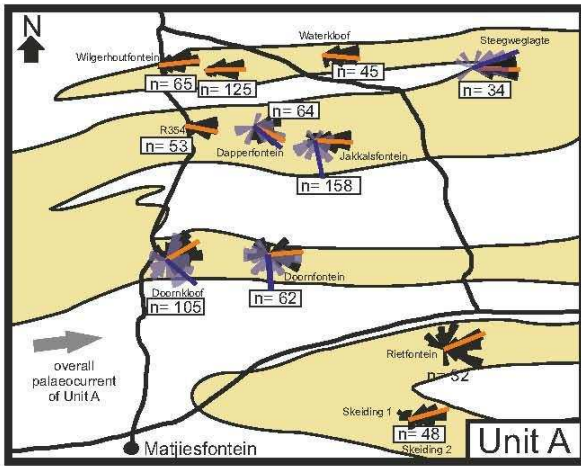
<b>Effects of tectonic shortening on estimated slope angles</b>					
<b>Subunits</b>	<b>A.1</b>	<b>A.2</b>	<b>A.3</b>	<b>A.5</b>	<b>A.6</b>
Current distance [m]	18682	18682	18682	18682	18682
Original distance [m] for 9.2% shortening	20401	20401	20401	20401	20401
Original distance [m] for 14.2% shortening	21335	21335	21335	21335	21335
Original distance [m] for 14.7% shortening	21428	21428	21428	21428	21428
Slope angle [°] with current distance	n.a.	0.03	0.05	0.33	0.01
Slope angle [°] (9.2% shortening)	n.a.	0.03	0.05	0.3	0.01
Slope angle [°] (14.2% shortening)	n.a.	0.03	0.05	0.29	0.01
Slope angle [°] (14.7% shortening)	n.a.	0.03	0.05	0.29	0.01











 mean palaeoflow direction lobes  
 mean palaeoflow direction slides

 palaeocurrents lobe facies  
 movement direction chaotic facies

10 km

